

# Complex wave fields in the interacting 1d Bose gas: when do they apply, and where to cut off the coherent region?

J. Pietraszewicz<sup>1</sup> and P. Deuar<sup>1</sup>

<sup>1</sup>*Institute of Physics, Polish Academy of Sciences, Aleja Lotników 32/46, 02-668 Warsaw, Poland*<sup>\*</sup>

(Dated: June 21, 2019)

We determine in detail the physical regimes for which the widely used matter wave (“c-field”) description is accurate in the interacting one-dimensional Bose gas. The whole range of interaction and temperature is covered. Results are given in terms of a figure of merit that bounds the discrepancy between classical wave fields and exact quantum predictions for many observables at once, as well as an optimal cutoff. The matter wave description is found to be good, below 10% error, in the entire quasicondensate region up to  $\gamma = g/n \approx 0.02$ , in the whole quantum turbulent regime, and in most of the degenerate gas up to  $T \approx 0.01 T_d$ . The energy cutoff found for the coherent subspace optimizes a broad range of observables. It usually depends only on temperature not density, making it universal for many cloud shapes. An exception is the coldest quantum fluctuating regime of  $k_B T \lesssim \mu$ , where it becomes density dependent. We find that the globally optimal cutoff is higher in energy than usually supposed. This high value is needed to obtain correct kinetic energy, but does not detrimentally affect other observables. Importantly, we show how the many earlier disparate results on the cutoff can be reconciled due to the weak cutoff dependence of some observables, and strong dependence of others – in a mini review.

## I. INTRO

The c-field description has become a ubiquitous and largely irreplaceable workhorse in the quantum gases community for dealing with a broad zoo of dynamical and thermal phenomena, particularly those that are non-perturbative or visible only in single experimental runs [1–16]. The idea is to treat the low energy part of the system as an ensemble of complex-valued wave fields like done in semiclassical quantum optics. There, when mode occupations are large, quantum electrodynamics of photons is very well approximated with classical electromagnetic fields. Hence the alternative name “classical fields”, though here for massive bosons they are in fact a *matter wave* field, and a deeply quantum phenomenon.

To say that a system’s state is well described by such matter waves implies a host of important physical consequences. Among them: The system behaves like a superfluid at least on short scales; Single realizations of the ensemble correspond to measurements of many particle positions in single experimental runs [1–3, 17–22]; All relevant features come from a collective contribution of many particles; Essentially nonperturbative phenomena such as quantum wave turbulence or self-organization can be present [16].

The field of quantum gases has seen a rapid growth of interest in these very kinds of phenomena as they have become accessible experimentally. Their study and comparison to experiment from the theoretical side has relied heavily and widely on the various flavors of classical field descriptions (GPE [3, 23–28], PGPE [1, 2, 29, 30], SGPE [17, 19, 31–33], SPGPE [34, 35], truncated Wigner [36–40]). This is because c-fields and vari-

ations around them are typically the only essentially non-perturbative treatment of quantum mechanics that remains tractable for very large systems. Examples of strongly non-perturbative effects that have been treated include: Defect seeding and formation [5, 7, 9, 15, 41–46]; Quantum turbulence [24, 47, 48]; The Kibble-Zurek mechanism [8, 49–52]; Nonthermal fixed points [53–56] and vortex dynamics [43, 57, 58]; The BKT transition [43, 59]; Evaporative cooling [7, 60, 61]; and more. Related effective field theories using complex-valued fields have been developed e.g. for polaritons [62, 63], superfluid Fermi gases [64–67] or for Yang-Mills theory [68].

In light of the fact that the approach has become so important in the community for dealing with these questions, it is very pertinent (and increasingly so) to pinpoint and understand the range of parameters for which matter wave physics is an adequate description. We do this here. The details allow us also to clarify a number of unresolved issues in the field.

The general understanding for the last 15 years or so has rested on two widely applicable qualitative arguments: Firstly, that the bulk of the physics must take place in single particle modes that are highly occupied. This allows one to neglect particle discretization and the non-commutativity of the Bose fields  $\hat{\Psi}(\mathbf{x})$  and  $\hat{\Psi}^\dagger(\mathbf{x})$ . Secondly, that the subspace of modes treated with c-fields should be limited to below some energy cutoff  $E_c$ , at which mode occupation is  $\mathcal{O}(1–10)$ . At this level particle discretization (which is impossible to emulate using a complex amplitude) becomes important. Such a cutoff also prevents the ultraviolet catastrophe that occurs because of the equipartition of  $k_B T$  energy per each mode in classical wave equilibrium. A substantial variety of prescriptions for choosing the cutoff have been obtained in the past, and are reviewed in Sec. VI. They differ significantly at the quantitative level, due to the disparate criteria used. Usually, they were tailored to correctly pre-

\* [pietras@ifpan.edu.pl](mailto:pietras@ifpan.edu.pl), [deuar@ifpan.edu.pl](mailto:deuar@ifpan.edu.pl)

dict one particular observable.

For a general treatment of a system with classical fields, however, one desires something broader: that at least all the usual measured observables are close to being described correctly. This is particularly important for the study of nonlinear dynamical and nonequilibrium phenomena such as quantum turbulence, or defect formation times, for which significant errors in one quantity will rapidly feed through into errors in all others. That is why it is essential that the description be correct for many quantities at once.

Our aim here is to quantitatively judge the accuracy of the c-field approach, circumscribe the parameters of the matter wave region, and reconcile the many cutoff prescriptions in a common framework so that calculations can be made with greater confidence in future. As we will show, the key to a better understanding is that some quantities are much more sensitive to cutoff than others, and that the dependence can be of two flavors.

In this paper we consider the one-dimensional Bose gas with repulsive contact interactions. To judge when matter wave physics is an accurate description, we construct a robust figure of merit. It is an upper bound on the discrepancy between the matter wave predictions and the exact quantum results for a set of the typical experimental observables. Once we obtain the dependence of this figure of merit on the cutoff, the choice that allows for the best overall treatment of the dynamics and observables will also become apparent. This follows the same tested route that was used in a preliminary study of the ideal Bose gas in [69]. There, importantly, two classes of observable dependence on the cutoff were identified, and kinetic energy was found to be the most sensitive observable. However, the classical wave and quantum results must be obtained with more advanced techniques here.

The procedure and assumptions are described in Sec. II, the limits of the matter wave region in Sec. III, and the resulting globally optimal cutoff in Sec. IV. Sec. V looks at some implications of these results (the occupation of the cutoff mode in Sec. VA, basic heuristic estimates in Sec. VB, consequences for dynamics in Sec. VC, and for nonuniform systems in Sec. VD). Sec. VI is a mini-review of the cutoff studies in the field to date, with comparison to the overall framework found here. We conclude in Sec. VII. The supplementary material gives additional detail on a number of matters [70].

## II. BACKGROUND AND TOOLS

### A. Classical wave fields

The classical field description of a system can be succinctly summarized as the replacement of quantum annihilation (creation) operators  $\hat{a}_k$  ( $\hat{a}_k^\dagger$ ) of single particle modes  $k$  in the second-quantized field operator by complex amplitudes  $\alpha_k$  ( $\alpha_k^*$ ). With mode wave functions

$\psi_k(\mathbf{x})$ , it can be written:

$$\hat{\Psi}(\mathbf{x}) = \sum_k \hat{a}_k \psi_k(\mathbf{x}) \rightarrow \Psi(\mathbf{x}) = \left\{ \sum_{k \in \mathcal{C}} \alpha_k \psi_k(\mathbf{x}) \right\}. \quad (1)$$

This is warranted when occupations are sufficiently macroscopic. Evidently, occupations will become *not* sufficiently macroscopic for modes with high enough energy. For this reason it is necessary to restrict the set of modes to a low energy subspace (often called the “coherent” or “c-field” region [1]), which is denoted by  $\mathcal{C}$ . This set is usually parametrized by a single cutoff parameter, at a given mode energy  $E_c$ . Note that, in general, the system’s state is represented using an ensemble  $\{\dots\}$  of complex field realizations, each with its own set of amplitudes  $\alpha_k$ . Each member breaks the gauge symmetry of a typical full quantum ensemble in a manner similar to single experimental realizations, but the ensemble preserves it [3, 22]. This naturally allows e.g. for the presence of spontaneous nonlinear many-body defects, and many interesting non-mean field phenomena that are very difficult to access using other approaches.

For in-depth discussion of the subject, we refer the reader to [1, 19, 22, 26] and the earlier reviews [2, 25, 33]. Dynamics is simulated with a Gross-Pitaevskii equation (GPE) or variants, whereas equilibrium ensembles can be obtained either in the long time ergodic limit of such simulations, or via more direct sampling of the thermal distribution. Details of our implementation are in supplementary material S1 [70].

C-field descriptions come in a variety of flavors, the most important difference for us here being whether the above-cutoff “incoherent” atoms are added to the description of the system or not. Addition was usually carried out using a Hartree-Fock (HF) approximation with non-interacting particulate atoms above the cutoff. While doing this adds to the model’s overall accuracy and weakens its sensitivity to the cutoff, the description is no longer cleanly in terms of matter waves and its accuracy cannot be used to make physical conclusions regarding whether the physics is that of matter-waves. For instance, the high temperature gas with particle-like physics is also described well with no c-field at all. For this reason, we will work here with the bare c-field description (1).

### B. Interacting 1d gas

We will consider the effectiveness of this classical wave physics for describing the one-dimensional Bose gas with repulsive contact interactions. This system underpins a very large part of ultracold gas experiment and theory, including the study of non-equilibrium physics, defects, turbulence, thermalization, and others. It is particularly suited to our study because of the existence of beautiful exact results for the uniform gas at arbitrary interaction strength due to Lieb and Liniger [71, 72] and arbitrary temperature due to Yang and Yang [73].

The gas's properties are encapsulated by two dimensionless parameters:

$$\gamma = \frac{mg}{\hbar^2 n}; \quad \tau_d = \frac{T}{T_d} = \frac{1}{2\pi} \frac{mk_B}{\hbar^2} \frac{T}{n^2}, \quad (2)$$

in terms of the density  $n$ , temperature  $T$ , particle mass  $m$ , and contact interaction strength  $g$ . (Provided there are no finite-size effects). The first parameter quantifies the interaction strength, moving from dilute Bose gases for  $\gamma \ll 1$  to a strongly interacting fermionized regime when  $\gamma \gg 1$ . The second one is a dimensionless temperature, in units of quantum degeneracy temperature  $T_d$  at which there is one particle per thermal de Broglie wavelength  $\Lambda_T = \sqrt{\frac{2\pi\hbar^2}{mk_B T}}$  in the ideal gas.

The parameter space of the system can be conveniently classified into a number of regions based on the behavior of density fluctuations [74–77]. For our purposes here, the relevant regions are:

- Classical gas:  $\tau_d \gtrsim 1/(4\pi)$  (physics generally described by classical particles, not waves);
- Quantum degenerate gas:  $\sqrt{\gamma} \lesssim 4\pi\tau_d \lesssim 1$  (Low energy modes occupied by more than one particle, density fluctuations large);
- Thermally fluctuating quasicondensate:  $\gamma \lesssim 4\pi\tau_d \lesssim \sqrt{\gamma}$  (phase coherence on appreciable scales, small density fluctuations dominated by thermal excitations, weak bunching of atoms);
- Quantum fluctuation dominated quasicondensate:  $4\pi\tau_d \lesssim \gamma \lesssim 1$  (phase coherence on long scales, small density fluctuations dominated by quantum depletion, weak antibunching);
- Fermionized gas:  $\gamma \gtrsim 1$  (physics dominated by strong interparticle repulsion, overlap between single-particle wavefunctions becoming small).

These regimes are all separated by crossovers.

### C. Analysis procedure

We proceed in a manner similar to a previous analysis of the ideal gas case [69].

#### 1. System and ensemble

Firstly, to obtain results reasonably independent of the trapping geometry, density profile, etc. we consider systems that are amenable to a local density approach (LDA). In this, it is assumed that the *ensemble averaged* density varies more slowly than other relevant physical quantities, and does not change over the size of the chosen section of the gas, of length  $L$ . This is sufficient to study defects and turbulence phenomena because it is only this averaged density that is assumed to vary slowly. The local density in a single realization can still vary strongly within the box.

For uniform systems, a basis of plane wave modes  $k \equiv \mathbf{k}$  is natural. The energy cutoff for the low energy subspace  $\mathcal{C}$  is equivalent to a momentum cutoff  $k_c$  so that only modes  $|\mathbf{k}| < k_c$  are included. Its dimensionless form using the same scale as  $\tau_d$  is

$$f_c = k_c \frac{\Lambda_T}{2\pi}, \quad (3)$$

which cuts at a kinetic energy of

$$\varepsilon_c = \frac{\hbar k_c^2}{2m} = \pi f_c^2 k_B T. \quad (4)$$

Working thus in the LDA with a uniform section of a larger gas, the grand canonical ensemble is the natural choice, as the rest of the system acts as a particle and thermal reservoir. This ensemble can be most readily obtained either by a Monte Carlo sampling as per [69, 78] or as the ergodic long-time limit of simulations using the SPGPE.

Results that are independent of finite-size effects are generally the most useful. We will impose the thermodynamic limit by using a box with periodic boundary conditions of a length  $L$  sufficiently large to contain the longest length scale in the system. Usually this is the phase correlation length, and is equivalent to requiring the first-order (“phase”) correlation

$$g^{(1)}(z) = \frac{1}{n} \langle \hat{\Psi}^\dagger(x) \hat{\Psi}(x+z) \rangle \quad (5)$$

to drop to zero when  $z \gtrsim L/2$ .

#### 2. Observables

For a correct treatment of the physics of the system, it is paramount that all the low order observables that form the staple of experimental measurements are calculated correctly, not just a chosen one or two. Further, for correct dynamics, the energy and energy balance (kinetic/interaction) must be correct. Any discrepancies here will rapidly feed through into the other quantities in a nonlinear system, whether in the form of energy mixing, or dephasing in integrable systems. For nonuniform systems, it becomes even more important as discrepancies in the density dependence of energy will immediately lead to bogus expansion or contraction.

For a general observable  $\Omega$ , let us define a relative discrepancy between the classical field value  $\Omega^{(cf)}$  and the true quantum one  $\Omega^{(q)}$ :

$$\delta_\Omega(\gamma, \tau_d, f_c) := \frac{\Delta\Omega}{\Omega} = \left( \frac{\Omega^{(cf)}(\gamma, \tau_d, f_c)}{\Omega^{(q)}(\gamma, \tau_d)} - 1 \right). \quad (6)$$

For an LDA treatment to make sense, it is of paramount importance that the density in the classical field matches the true value  $n$ , otherwise the whole match will be awry.

Hence, we always compare exact and classical field ensembles having the same ensemble-averaged density, so that  $\delta_n = 0$  by construction. In what follows, for a given interaction strength  $g$  and temperature  $T$ ,  $\delta_n = 0$  is equivalent to matching our physical parameters  $\gamma$  and  $\tau_d$  (2) with  $\gamma^{CF}$  and  $\tau_d^{CF}$  characterizing the *CF* system. This step leaves one free parameter  $f_c$  in the classical field description whose value could be chosen to make one other observable agree exactly. Such an approach has been used for most cutoff benchmarking in the past. However, a good classical wave description will only be present if there is some cutoff choice that leads to small discrepancy  $\delta$  in *all* the relevant observables simultaneously.

In a previous study [69], the dependence of the discrepancies on cutoff was analyzed, and one of the most important results was that **observables fall into two broad categories**. These categories are confirmed here in the interacting gas – see Figs. 1 and 3.

The first kind of observable is overestimated for small cutoffs ( $\delta_\Omega > 0$ ). Their discrepancy falls with  $f_c$  and then usually attains negative values. This group includes such quantities as the half-width of the  $g^{(1)}(z)$  correlation function (i.e. the phase coherence length) and values of  $g^{(1)}(z)$  at large distances  $z$ , the condensate fraction  $n_0$ , the effective temperature in a microcanonical ensemble [30, 79], or the coarse grained density fluctuations. These last are given by

$$u_G := \frac{\text{var} \hat{N}}{\langle \hat{N} \rangle} = S_0 = n \int d\mathbf{z} [g^{(2)}(\mathbf{z}) - 1] + 1 \quad (7)$$

and will play an important role below. This quantity is also known as the  $k = 0$  static structure factor  $S_0$ . It is the ratio of the measured number fluctuations to Poisson shot noise in regions that are wider than the density correlation length, and serves as a measure of the typical number of particles per randomly occurring density lump. It tends (i) to 1 in a coherent state or at high temperature, (ii) to zero at  $T = 0$  or in a fermionized gas, and (iii) to large positive values in the thermal-dominated quasicondensate. It is a density fluctuation quantity that is quite readily measured in experiments (e.g. [80–85]) because standard pixel resolution is sufficient, and is an intensive thermodynamic quantity. These features are to be contrasted to the microscopic density-density correlation  $g^{(2)}(z) = \langle \hat{\Psi}^\dagger(x) \hat{\Psi}^\dagger(x+z) \hat{\Psi}(x+z) \hat{\Psi}(x) \rangle / n^2$ , to which it is related by (7)!

The second category of observables follows the opposite trend, being underestimated for low cutoff, but eventually attaining positive discrepancy  $\delta$ . The most prominent example are energies per particle, particularly the kinetic energy per particle,  $\varepsilon$ . Others are some collective mode frequencies in a trap [86], and  $g^{(2)}(0)$  in the interacting gas. The density  $n$  also behaves this way when changing only  $k_c$ , but is guaranteed matched in our approach.

In the ideal gas, the observables from the two classes above with the most disparate behavior are the coarse-

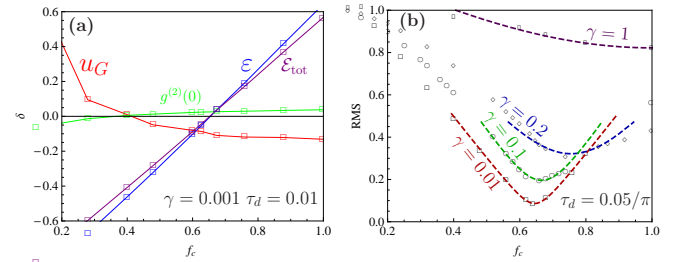


Figure 1. Example of accuracy assessment for a particular choice of parameters. Panel (a): cutoff dependence of the discrepancies  $\delta$  of single observables for the case  $\gamma = 0.001$ ,  $\tau_d = 0.01$ .  $g^{(2)}(0)$  (green),  $u_G$  (red),  $\mathcal{E}_{\text{tot}}$  (purple), and  $\varepsilon$  (blue). Panel (b): cutoff dependence of the global discrepancy  $RMS(f_c)$  at  $\tau_d = 0.0159$  obtained numerically for several values of  $\gamma$ : 0.01 (square), 0.1 (circle), 0.2 (diamond), 1 (rectangle). Dashed curves show the fit (parabolic to  $(RMS)^2$ ) to numerical points near the minimum.

grained density fluctuations  $u_G$  and kinetic energy  $\varepsilon$  [69]. Their mismatch turned out to be the strongest restriction on the range of  $f_c$  for which all  $\delta_\Omega$  errors are small. Based on this, a global figure of merit was defined for the ideal gas which comprised the root mean square of the discrepancies in these two observables:  $RMS_{\text{id}} = \sqrt{\delta_\varepsilon^2 + \delta_{u_G}^2}$ . This had the convenient property of an upper bound on the discrepancy of any of the other observables. In the matter wave region where  $RMS$  is small, kinetic energy is the observable that is the most strongly sensitive to cutoff. This will be particularly important later when dynamics is considered.

For the interacting gas one should include the total energy per particle  $\mathcal{E}_{\text{tot}}$ , and interaction energy in the analysis. Neither of these was relevant for the ideal gas.

The behavior of discrepancies for a number of important observables is shown in Fig. 1(a) and 3(a,c). One sees the same trends as for the ideal gas for the pertinent observables, while the discrepancies in the total energy and interaction energy (proportional to  $g^{(2)}(0)$ ) grow with  $f_c$ , albeit slower than  $\varepsilon$ . Similar trends are seen for other values of the parameters  $\gamma$  and  $\tau_d$  (see also Fig. S3 in the supplementary material [70]).

In this work consideration was also given to the condensate mode occupation,  $N_0$ , i.e. the number of atoms with  $k = 0$ . This observable tends to a well defined constant value as the gas length grows, but of course it becomes negligible compared to  $N$  in the thermodynamic limit of the 1d gas.  $N_0$  will be important later for comparison to earlier cutoff determinations which were often made in low temperature mid-size systems with  $\mathcal{O}(1000)$  atoms, where condensate fraction  $n_0$  remained significant.

### 3. Figure of merit

To carry over the interpretation of our figure of merit as a root-mean-square upper limit on observable discrepancies from the ideal to the interacting gas, it is necessary to include discrepancies of both the total energy per particle  $\mathcal{E}_{\text{tot}}$  and the kinetic energy  $\varepsilon$ . A correct total energy density is essential for accurate dynamics, while the kinetic energy density is closely related to phase coherence length, and the momentum distribution.

One could ask also about the interaction energy per particle  $\mathcal{E}_{\text{int}} = \frac{1}{2}gn g^{(2)}(0)$ . We find that it is more weakly dependent on cutoff than the total energy, at least for the physical regimes in which  $RMS$  is small. Fig 1(a) and 3(a,c) show this using  $g^{(2)}(0)$ . We did not investigate its dependence at large  $\gamma$  where the accuracy of the classical field for the other observables above is poor, regardless of what happens with the interaction energy. The overall conclusion is that  $\mathcal{E}_{\text{int}}$  can be omitted from the figure of merit without loss of generality. The discrepancy in  $N_0$  turns out to be smaller than that of  $\mathcal{E}_{\text{tot}}$  and/or  $u_G$  in the cases we considered.

The measure of global error (at a given cutoff) that results from these considerations is

$$RMS(\gamma, \tau_d, f_c) = \sqrt{\left(\delta_{u_G}\right)^2 + \max\left[\delta_\varepsilon^2, \delta_{\mathcal{E}_{\text{tot}}}^2\right]}. \quad (8)$$

We use the maximum of the energy discrepancies rather than an rms of all three potentially extreme observables because this has a more convenient interpretation in the high temperature and the ideal gas regimes, when  $\mathcal{E}_{\text{tot}} = \varepsilon$ . The maximum is desirable because (1) we do not wish to double count the importance of energy to keep the interpretation of  $RMS$  as being close to the upper bound on the discrepancy (not  $\sqrt{2}$  times the upper bound), and (2) to remain consistent with the ideal gas results of [69]. The dependence of (8) for a variety of cases is shown in Figs. 1(b) and 3(b,d).

We find the minimum of this global error quantity to determine the best that one can do ( $\text{min}RMS$ , which will be our figure of merit for the classical field description), and the best cutoff to use (which we will call  $\text{opt}f_c$ ).

## III. THE CLASSICAL WAVE REGIME

The dependence of the figure of merit  $\text{min}RMS$  on physical parameters  $\gamma, \tau_d$  is shown in Fig. 2 as a contour plot. Recall – errors in all typical observables are smaller than this contour value. Knowing that experimental uncertainties are typically of the order of 10%, a value of  $\text{min}RMS \leq 0.1$  tells us that in practice the physics in this region is the physics of classical matter wave fields.

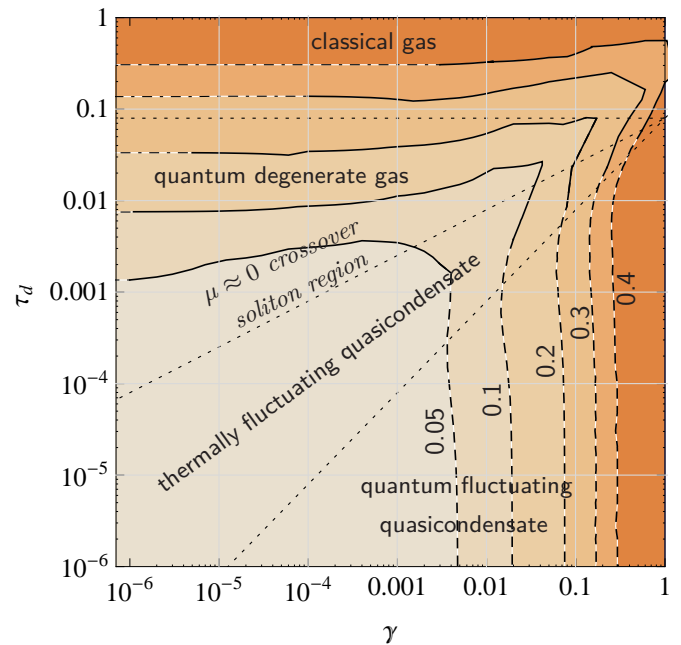


Figure 2. The regime of applicability for classical wave fields. Contours of the figure of merit (upper bound on discrepancy of observables) are shown at values of  $\text{min}RMS$  indicated on the plot. The contours drawn with solid lines come from numerically generated classical field ensembles, while the dashed lines are obtained with the extended Bogoliubov theory of [87]. Dot-dashed lines are interpolations to ideal gas values obtained in [69]. Dotted lines indicate crossovers between physical regimes, as per Sec. II B. For more technical details, see Fig. S4(a) [70].

### A. Ensembles

Details of how the values of  $RMS$ ,  $\text{min}RMS$ , and the contours are obtained are given in the supplemental material [70]. In brief:

(i) To obtain classical field ensembles for the hotter temperatures in the diagram, we chose a scattering of points (see Fig. S1 [70]) in the  $\gamma, \tau_d$  parameter space. For each choice of a  $\gamma, \tau_d$  pair, we generated a series of c-field ensembles for various values of  $f_c$ . These were used to generate observable estimates, discrepancies  $\delta_\Omega(\gamma, \tau_d, f_c)$ , and  $RMS(\gamma, \tau_d, f_c)$ , by comparing to the exact Yang-Yang values. Most ensembles were generated using a Metropolis algorithm for a grand canonical ensemble as described in [69], based on the earlier work of [78]. For a few locations in the large  $\gamma$ , low  $\tau_d$  region where this method was very inefficient, the ensemble was generated by the equivalent method of evolving an SGPE to its stationary ensemble.

(ii) For the above ensembles, the exact quantum values of observables  $\mathcal{E}_{\text{tot}}, N$  are obtained as described in [73],  $\varepsilon$  can be calculated from the Yang-Yang solution using the above, and  $g^{(2)}(0)$  as per [74, 75]. The  $u_G$  calculation uses a specially developed method [88], summarized in the supplement S2 [70].

(iii) For the coldest temperatures, especially when  $\tau_d \lesssim \gamma$ , the above methods become very inefficient (slow convergence and/or increasing difficulty in removing finite-size effects). Instead, we used the quasicondensate Bogoliubov theory of Mora and Castin [87] to calculate both the full quantum and the corresponding c-field predictions. See supplement S3 for details and Fig. S2 for the region in which the Bogoliubov theory is accurate [70].

Separate sets of contours were generated based on the numerical ensembles and the Bogoliubov results, as shown in Fig. S4 [70]. The match was excellent in the overlap region where both apply. Fig. 2 shows a synthesis of the above determinations, where only the most accurate data for a given  $\gamma, \tau_d$  pair are used.

In the supplement one can find further details such as how the density  $n$  and chemical potentials  $\mu$  between c-field and exact results were matched (Sec. S2), how the data was fitted to obtain  $\text{minRMS}$  and  $\text{opt}f_c$  (Sec. S4), or how contours were interpolated (Sec. S4B). Fig. S5 shows cuts of the  $\text{minRMS}$  dependence on  $\gamma$  and  $\tau_d$ .

## B. Remarks

Let us make some initial remarks on the results of Fig. 2 (further analysis will ensue in Sec. V).

All in all, the region dominated by classical wave physics is larger than one could have conservatively supposed. Firstly, we see that essentially the entire quasicondensate regime is described well in terms of our macroscopic observables, for the whole range of temperatures, and all the way until the crossover to fermionization kicks in around  $\gamma = 0.018$  to  $0.075$ . (The values quoted correspond to discrepancies  $\text{minRMS} = 0.1$  and  $0.2$ , respectively).

Importantly, all mentioned observables remain well described even in the colder quantum-dominated quasicondensate down to  $T = 0$ , which is not obvious *a priori*. We know that the weak antibunching that occurs here due to quantum depletion ( $g^{(2)}(0) \approx 1 - 2\sqrt{\gamma}/\pi$  [76, 77]) cannot be correctly replicated by classical fields. However, this clearly has little effect on any of the main observables and even on the density fluctuation statistics described by  $u_G$ . The reason for this fortuitous circumstance lies in the fact that the two contributions to  $u_G$  in (7) that are missing in classical fields (shot noise “+1” and antibunching in  $g^{(2)}$ ) cancel in the full quantum description when temperature drops. In the c-field description,  $n_{\text{cf}} = \frac{1}{L} \int dx |\Psi(x)|^2$ ,  $g_{\text{cf}}^{(2)}(z) = |\Psi(x)|^2 |\Psi(x+z)|^2 / n_{\text{cf}}^2$  and the number fluctuations are related by

$$u_G^{\text{cf}} := n_{\text{cf}} \int d\mathbf{z} [g_{\text{cf}}^{(2)}(\mathbf{z}) - 1]. \quad (9)$$

The shot noise “+1” term is no longer present, and values of  $u_G$  tending to zero can continue to be obtained despite  $g_{\text{cf}}^{(2)}(z) > 1$ . The dependence of observables and their discrepancy in the quasicondensate regime is shown

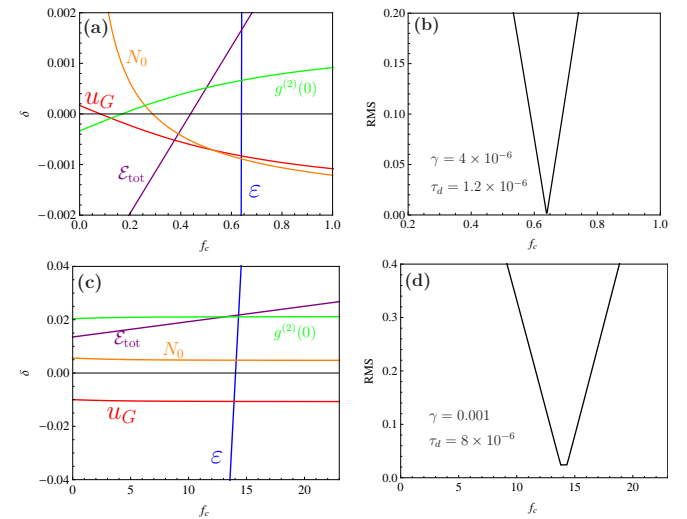


Figure 3. Cutoff dependence in the quasicondensate. The top panels are in the thermally dominated regime  $\gamma = 4 \times 10^{-6}$ ,  $\tau_d = 1.2 \times 10^{-6}$ , and the lower panels in the quantum fluctuation regime  $\gamma = 10^{-3}$ ,  $\tau_d = 8 \times 10^{-6}$ . Notation is as in Fig. 1, with the additional observable  $N_0$ , the atom number in the condensate mode  $k = 0$  (orange lines). Left panels: discrepancies for single observables calculated with the extended Bogoliubov [87]; Right panels: global discrepancy  $\text{RMS}$ .

in Fig. 3. The plateau in the dip in panel (d) is a real effect, and arises because  $\mathcal{E}_{\text{tot}}$  is only weakly dependent on cutoff. Details can be found in Sec. S6 and Fig. S3 [70].

The great majority of the decoherent regime is correctly described, including all temperatures up to at least  $\tau_d \approx 0.008$  ( $\text{minRMS} = 0.1$ ) and  $0.03$  ( $\text{minRMS} = 0.2$ ). This is a second important result, as it is not immediately obvious that classical fields apply so far into the high temperature regime. What this means is that not only do they cover the entire quasicondensate regime but a number of strongly fluctuating higher temperature regimes as well. The regime described in [9, 89] with prominent thermal solitons (in the range  $\tau_d \sim 0.04\sqrt{\gamma} - 0.2\sqrt{\gamma}$ ) is treated well (see Fig. 2). At warmer temperatures  $\tau_d \approx 0.27\sqrt{\gamma}$ <sup>1</sup>, the crossover regime to an ideal-gas-like state that occurs when  $\mu$  changes sign and can be described by a Hartree-Fock model [90] also lies well within the classical wave region. In particular, this means that the changeover from wave-like to particle-like physics occurs at much higher temperatures than the crossover between Bogoliubov and Hartree-Fock physics.

The above two regimes lying near  $\tau_d \sim 0.1\sqrt{\gamma}$  are well described by matter waves even for a range of stronger interactions  $\gamma$  than found for hotter or colder systems. This is the wedge of low  $\text{RMS}$  values along the dotted  $\tau_d \propto \sqrt{\gamma}$  line in the region of  $\tau_d \approx 0.01$ ,  $\gamma \approx 0.02$  in

<sup>1</sup> Obtained from exact Yang-Yang calculations [73].

Fig. 2. The reason for this “salient” is not understood at the moment.

Finally, observing the left edge of Fig. 2, we can confirm that our numerical results for  $\text{minRMS}$  match well to the ideal gas results of [69] since the dot-dashed interpolations are horizontal.

#### IV. THE GLOBALLY OPTIMAL CUTOFF

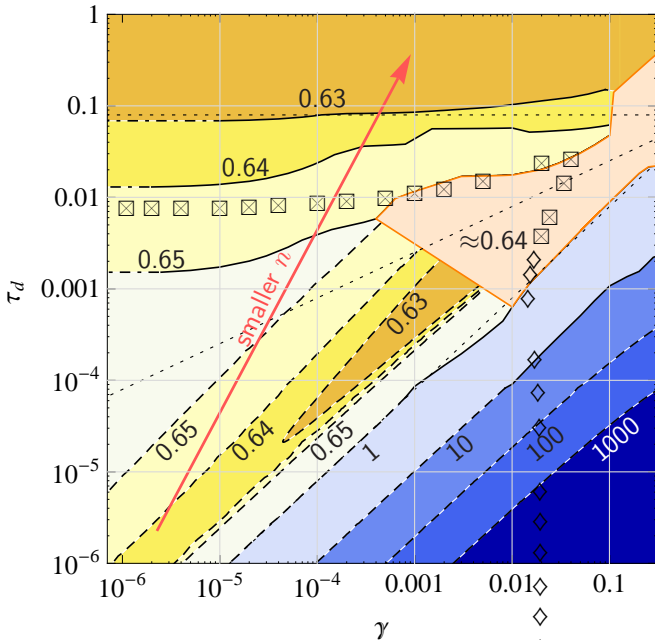


Figure 4. Globally optimal values of the cutoff  $\text{opt}f_c$ , shown with contours. Notation as in Fig. 2, contour values are on the plot. For reference, black symbols show the location of  $\text{minRMS} = 0.1$  from Fig. 2 obtained with Metropolis (squares) and Bogoliubov [87] (diamonds). The salmon colored area indicates a region with  $\text{opt}f_c \approx 0.64$  in which there was a insufficient precision in the numerical ensembles to determine the position of the closely spaced contours. The arrow shows decreasing density with constant  $T$  and  $g$  and is discussed in Sec. V D. For technical details, see Fig. S4(b) [70].

Figure 4 shows the dependence of the optimal cutoff parameter  $\text{opt}f_c$  as a contour plot. The main standout feature is the presence of two regions for  $\text{opt}f_c$  with a transition between them at  $\tau_d \approx 0.1\gamma$ . In the higher temperature regime, a constant  $\text{opt}f_c \approx 0.64$  is a very good approximation, while in the very low-temperature regime, cutoff grows rapidly according to (11). The  $\text{opt}f_c$  incorporates the basic temperature dependence  $k_c \propto \text{opt}f_c \sqrt{T}$  and  $\varepsilon_c \propto (\text{opt}f_c)^2 T$  as per (3–4), and matches the figure of merit in Fig. 2.

#### A. Thermal region with constant cutoff

The constant-cutoff region closely matches the regimes in which fluctuations are mainly thermal (quasicondensate or otherwise), while the high-cutoff region is the quasicondensate dominated by quantum fluctuations. The changeover is around  $\tau_d \approx \gamma/2\pi$ , parallel and just above the  $\text{opt}f_c = 1$  contour on the plot. In the quasicondensate regime, one has  $\mu \approx gn$ , which means that this changeover occurs at  $k_B T \approx \mu$ .

We can state then, that in systems for which the matter wave description is at all correct ( $\text{minRMS} \lesssim 0.2$ ) and  $k_B T \gtrsim \mu$ , there is a universal optimum dimensionless cutoff

$$\text{opt}f_c = 0.64 \pm 0.01 \quad (10a)$$

i.e.

$$k_c = (1.60 \pm 0.03) \frac{\sqrt{m k_B T}}{\hbar}; \quad \varepsilon_c = (1.29 \pm 0.04) k_B T. \quad (10b)$$

We note also that the extended Bogoliubov analysis [87] used for most of the thermal quasicondensate shows a very shallow and broad trough with  $\text{opt}f_c$  values down to  $0.63 - 0.62$ , which occurs for  $\tau_d \approx \gamma$ . As far as we can tell, it does not have any important consequences because choosing  $\text{opt}f_c = 0.64$  instead gives practically the same discrepancies and  $RMS$ .

These results are in agreement with the earlier work of [69]. The ideal gas limit  $\gamma \rightarrow 0$  matches as seen in Fig. 4, while the constant behavior in the interacting gas seen there for  $\tau_d = 0.00159$  and  $\gamma < 0.005$  was completely within the constant- $\text{opt}f_c$  region. Importantly, we confirm here that  $\text{opt}f_c$  is basically constant, and the cutoff  $k_c$  has only the standard  $\sqrt{T}$  temperature scaling across this whole broad swath of interacting gases. The ideal gas low-temperature limit that applies for small  $\gamma$ , and broadly for the whole region can be found exactly by the methods of [69], and is  $\text{opt}f_c \rightarrow \zeta(3/2)/4 = 0.653$ . This implies that the low- $\gamma$  part of Fig. 4 and regions to the left are very flat.

#### B. Quantum fluctuating region

Now the cutoff dependence in the other, ultra-low temperature regime,  $k_B T \lesssim \mu$ , can be obtained from the Bogoliubov description [87]:

$$\text{opt}f_c = \frac{1}{12\pi^2} \left( \frac{\gamma}{\tau_d} \right)^{\frac{3}{2}} \left\{ 1 - \frac{7\sqrt{\gamma}}{2\pi} + \frac{3\pi^2 \tau_d}{\gamma} + \dots \right\}. \quad (11)$$

Here  $2\pi\tau_d \ll \gamma \lesssim 1$ . The corresponding figure of merit is

$$\text{minRMS} = \frac{\sqrt{5\gamma}}{\pi} \left[ 1 + \frac{\sqrt{\gamma}}{30\pi} + \pi^2 \frac{\tau_d}{\gamma} + \dots \right]. \quad (12)$$

Sec. S6 gives more detail and higher order terms [70]. The exact dependence from numerics is shown in Fig. 5.

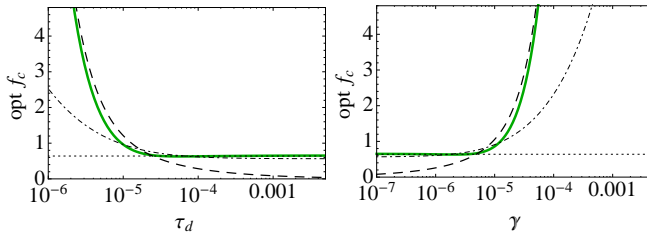


Figure 5. Optimal cutoff shown for two characteristic slices in parameter space (in green). Left panel:  $\gamma = 1.2 \times 10^{-4}$ . Right panel:  $\tau = 10^{-6}$ . The black lines show the two approximations discussed in the text: (10) – (dotted), (11) – (dashed), as well as the hitherto “rule of thumb” (13) (dot-dashed).

We can compare (11) to the widely used “rule of thumb” for the energy cutoff [2, 22, 91, 92]:  $\varepsilon_c \approx k_B T + \mu$ . In the quasicondensate regime, this cutoff corresponds to

$$f_c \approx \sqrt{\frac{1}{\pi} \left( \frac{\gamma}{2\pi\tau_d} + 1 \right)} \quad (13)$$

with  $\mu \approx gn = \gamma k_B T / 2\pi\tau_d$ , and the scaling (4). Note that (13) and (11) depend primarily on the ratio  $\gamma/\tau_d$ . Both grow with this quantity when  $k_B T \ll \mu$ , but the global  $\text{opt } f_c$  grows with a faster power law. The difference can be seen in Fig. 5.

The growth of  $f_c$ , and the different scaling warrants investigation. In Fig. 3(c) we can see that the high value of the cutoff given by (11) is necessary to obtain the correct kinetic energy. Moreover, the value given by the rule of thumb (here  $f_c = 2.58$ ) is far too small and gives a -93% discrepancy in  $\varepsilon$ . Other observables care rather little about the cutoff value in this regime. This has been noted previously e.g. for  $g^{(1)}$  and  $g^{(2)}$  [93].

If we consider length scales for the low energy subspace, then a basic requirement would be to resolve the healing length  $\xi = \hbar/\sqrt{m\mu}$  [93]. The smallest length scale accessible with a  $k_c$  cutoff in a plane wave basis is about half of the wavelength  $\lambda_c = 2\pi/k_c$ . In the quantum fluctuation region when  $\mu \gg k_B T$ ,  $\lambda_c/2 \approx 3\pi(\frac{k_B T}{\mu})\xi$  using the globally optimized cutoff (11) and  $\lambda_c/2 = \frac{\pi}{\sqrt{2}}\frac{1}{\sqrt{1+k_B T/\mu}}\xi \approx \frac{\pi}{\sqrt{2}}\xi$  using the rule of thumb (13). This shows that the rule of thumb is basically equivalent to allowing length scales down to  $\xi$ , while the correct rendering of the kinetic energy given by  $\text{opt } f_c$  requires us to allow also for much smaller length scales. Interestingly, Fig. 3(c) as well as the small value of  $\text{minRMS}$  at  $\text{opt } f_c$  indicate that the relatively very high cutoff does not introduce any deleterious side-effects in other observables, at least in this regime.

The reason why such a high cutoff is needed to get the right kinetic energy is that this quantity begins to rise steeply with  $\gamma$  when  $2\pi\tau_d \ll \gamma \ll 1$ , as shown in Fig. S6 [70]. In Sec. S6 we find that  $\varepsilon \approx \frac{k_B T}{6\pi^2} \frac{\gamma^{3/2}}{\tau_d}$ . The growing kinetic energy is contained in repulsive quantum fluctuations that go on to support fermionization when

$\gamma$  exceeds one. In a c-field description one should introduce more particle-like modes (each mode holds  $k_B T$  energy) to build up the kinetic energy to the right amount and compensate the lack of quantum fluctuations. Since the particle-like modes have very little occupation in this regime, other observables are practically unaffected, at least in 1d. This is discussed in more detail in Sec. S5 [70].

To conclude this section, we note that the transition to higher temperatures occurs near  $\mu = k_B T$  in both the optimized cutoff (11) and the rule of thumb (13). The latter tends to a value of  $f_c \approx 1/\sqrt{\pi} = 0.564$  which is somewhat too low, leading to an error in kinetic energy of about -20% that can be spotted in Figs. 1(a) and 3(b).

## V. FURTHER ANALYSIS

### A. Cutoff mode occupation

In the history of the subject, the cutoff has typically been given either in terms of the kinetic energy  $\varepsilon_c$  (and wavevector  $k_c$  related by (4)), or in terms of the c-field occupation  $N_c = \langle |\alpha_{|k|=k_c}|^2 \rangle$  of the (quasi)particle modes with highest energy  $E_c$ . One has  $N_c = k_B T / (E_c - \mu)$  in classical field equilibrium.

These two kinds of quantity are related, but not in a trivial way. For example for free particle modes in equilibrium, clearly

$$N_c \approx \frac{k_B T}{\varepsilon_c} = \frac{1}{\pi(\text{opt } f_c)^2}, \quad (14)$$

but in a Bogoliubov quasiparticle treatment the relationship is more involved. The excitation energy at wavevector  $k_c$  is then  $E_c - \mu = \sqrt{\varepsilon_c(\varepsilon_c + 2\mu)}$ , which is  $\gg \varepsilon_c$  at low temperatures  $k_B T \ll \mu$ . This causes that the quasiparticle occupation at  $k_c$  is much smaller than the ideal gas expression (14).

It is of much interest to find the values  $N_c$  at the optimum cutoff  $\text{opt } f_c$  and to see whether they are approximately constant and  $\mathcal{O}(1)$ , as has usually been assumed. Fig. 6 shows this – the mean occupation of the highest energy mode in the classical field when the cutoff is given by the global  $\text{opt } f_c$ . In the low-temperature ideal gas,  $N_c = k_B T / \varepsilon_c = 1/\pi(\text{opt } f_c)^2 = 0.746$ .

The obvious comment resulting from Fig. 6 is that while the expected constant  $\mathcal{O}(1)$  values of  $N_c \approx 0.746$  occur in the thermal region,  $N_c$  plummets to zero in the quantum fluctuating regime of  $k_B T \ll \mu$ . In fact, the low  $T$  behavior is

$$N_c = 18 \left( \frac{2\pi\tau_d}{\gamma} \right)^3 \left[ 1 + \frac{7\sqrt{\gamma}}{\pi} - \frac{6\pi^2\tau_d}{\gamma} + \dots \right] \approx 18 \left( \frac{k_B T}{\mu} \right)^3 \quad (15)$$

by a simple application of (11) and the Bogoliubov spectrum.

Less obviously, plummeting values of  $N_c$  are also implied by the rule of thumb (13), only that the fall is

somewhat less steep:  $N_c \approx \frac{1}{\sqrt{3}}k_B T/\mu$ . It follows that, when  $\mu \ll k_B T$ , small occupations of the cutoff mode are needed even to access the essential healing-length scale. It is merely that even smaller ones are necessary to get the kinetic energy right.

Yet, it seems remarkable that in this regime the time-honored intuition of  $\mathcal{O}(1)$  cutoff mode occupation can be discarded without any effect on the other observables. It is, however, convenient: Many studies that use the GPE in very low temperature regimes have used very high resolution numerical grids, and it is gratifying to know that most observables are not appreciably distorted by such a procedure.

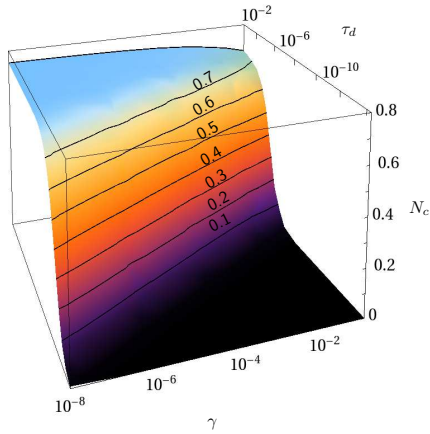


Figure 6. Occupation of the highest energy mode  $N_c$  when the cutoff is given by the globally optimized  $\text{opt } f_c$ . Black lines show contours with spacing of 0.1. The value at low  $\gamma$  and high  $\tau_d$  is 0.746.

## B. The boundaries of the matter wave regime

Some useful analytical approximations regarding  $\text{opt } f_c$  and  $\text{minRMS}$  are readily obtained.

We know already that the optimum cutoff is basically unchanged in the entire thermal-dominated region and it coincides with the ideal gas result from [69]. Let's revisit this ideal gas paper (especially the top row of its Fig. 2), where the discrepancy in  $u_G$  becomes very flat at low temperatures for a wide range of  $f_c$ , while the discrepancy in  $\varepsilon$  remains always highly sensitive.

The quantum prediction for  $\varepsilon$  in the thermodynamic limit  $L \rightarrow \infty$  at  $\gamma = 0$  is

$$\varepsilon^{(q)} = \frac{1}{2\pi n} \int_{-\infty}^{\infty} dk \frac{\hbar^2 k^2}{2m} n_k^{(q)} \quad (16)$$

with Bose-Einstein mode occupations  $n_k^{(q)} = [e^{(\hbar^2 k^2/2m - \mu)/k_B T} - 1]^{-1}$ , while the corresponding c-field quantity uses the cutoff  $f_{-k_c}$  and Rayleigh-Jeans occupations from equipartition:  $n_k^{(\text{cf})} = k_B T/(\hbar^2 k^2/2m - \mu)$ .

The above and a similar calculation for  $u_G$  give:

$$\delta_\varepsilon = \frac{4f_c}{\zeta(\frac{3}{2})} - 1 + \mathcal{O}(\tau_d^{\frac{1}{2}}); \quad \delta_{u_G} = \sqrt{\tau_d} \left[ \frac{6}{f_c \pi} + 3\zeta(\frac{1}{2}) \right] + \mathcal{O}(\tau_d) \quad (17)$$

In fact, this kind of behavior is typical for a wide range of parameters not just the ideal gas – e.g. see Fig. 1(a) and 3 here. Analysis of (17) shows that no positive  $f_c$  value can satisfy  $\delta_{u_G} = 0$ . In effect for low  $\tau_d$ , the kinetic energy  $\varepsilon$ , and the location of  $\delta_\varepsilon = 0$  set the optimal cutoff value. Using (17) leads to the usual ideal gas cutoff result  $k_c = \frac{\zeta(3/2)}{4} \sqrt{\frac{2\pi k_B T m}{\hbar^2}}$ , i.e.

$$\text{opt } f_c \approx \frac{\zeta(\frac{3}{2})}{4} \approx 0.653. \quad (18)$$

At this approximate optimal point, the  $\delta_{u_G}$  expression in (17) gives an estimate of  $\text{minRMS}$ . Solving for  $\tau_d$  one obtains  $\tau_d \approx (\text{minRMS})^2 / [\frac{24}{\pi \zeta(\frac{3}{2})} + 3\zeta(\frac{1}{2})]^2$ . The estimated values of  $\tau_d = 0.0047$  and  $0.019$  for the location of  $\text{minRMS} = 0.1$  and  $0.2$ , respectively, are relatively close to the actual numerical values.

Fig. 2 shows that the high- $\tau_d$  limit of the matter-wave regime is practically independent of  $\gamma$  for  $\gamma \lesssim 0.001$ . Accuracy better than 10% reaches  $\tau_d \lesssim 0.008$ , and the “wedge region” reaches  $\tau_d \approx \gamma \approx 0.03$ . For the more lenient  $\text{minRMS} \lesssim 0.2$ , the numbers are  $\tau_d \lesssim 0.033$  at low  $\gamma$  and  $\tau_d \approx 0.08, \gamma \approx 0.15$  in the wedge.

From the strongly interacting side, the limit of the matter wave regime lies around  $\gamma \lesssim 0.02$  for  $\text{minRMS} = 0.1$  and  $\gamma \lesssim 0.08$  for  $\text{minRMS} = 0.2$ . It turns out that this limit has a fairly simple explanation. In the quantum dominated quasicondensate ( $\tau_d \ll \gamma$ ), energy is dominated by interaction energy, and this quantity is proportional to  $g^{(2)}(0)$ , which is less than unity. However – in the c-field description,  $g^{(2)}(0)$  cannot be less than one, so we expect there to be at least a  $(1 - g^{(2)}(0))$  error in energy that cannot be alleviated by any choice of cutoff. Hence,  $\text{minRMS} \geq (1 - g^{(2)}(0))$ . Using approximate expressions for  $g^{(2)}(0)$  from [76], one obtains the estimate

$$\text{minRMS} \geq \frac{2\sqrt{\gamma}}{\pi} \left[ 1 - \frac{1}{3} \left( \frac{\pi^2 \tau_d}{\gamma} \right)^2 \right]. \quad (19)$$

The temperature-dependent term is negligible in the relevant region, and the location of the end of the matter-wave region lies at

$$\gamma = \frac{g}{n} \approx \left( \frac{\pi \text{minRMS}}{2} \right)^2. \quad (20)$$

The estimate (20) gives  $\gamma = 0.025$  for  $\text{minRMS} = 0.1$  and agrees very well with the values obtained numerically.

## C. Equilibrium and dynamics

Most previous cutoff determinations were based on static observables such as condensate fraction  $n_0$  or its

distribution, correlations  $g^{(1)}$  or  $g^{(2)}(0)$ , density  $n$ , or the effective temperature. These quantities, maybe apart from temperature, tend to be dominated by the most classical, highly occupied modes.

In comparison, the high-energy low-occupied modes have a much larger relative importance for determining the energy (especially kinetic energy  $\varepsilon$ , due to its  $k^2$  weighting of modes). The discrepancy  $\delta_\varepsilon$  tends to be more sensitive to  $f_c$  than the others, and the cutoff that correctly matches  $\varepsilon$  tends to lie higher in energy. The equal importance of kinetic energy here is the operational reason that the multi-observable cutoff  $\text{opt } f_c$  is at a higher energy than in most previous determinations.

What we have shown here, firstly, is that the description of the other observables is not adversely affected even with the somewhat higher cutoff  $\text{opt } f_c$ . Since  $\text{minRMS}$  remains small, then from its definition, the discrepancies  $\delta_\Omega$  stay small as well, which is confirmed by Figs. 1 and 3. On the other hand, the error in kinetic energy from cutoffs proposed in the past is large, and  $\varepsilon$  can be off by a factor of several for the more severe cases. What was not noted before is that the modes that contribute most to  $\varepsilon$  are not the same that contribute most to the majority of the other observables. As a result, errors in one set of observables in equilibrium are not strongly correlated with errors in the other set.

However, for an accurate treatment of *dynamics* in a nonlinear system, correct energies become crucial. This is because errors in energy in one part of the system rapidly infect the rest of the system with errors through the nonlinearity. This is going to be particularly evident in a nonuniform cloud where incorrect energy density in one region will lead to spurious movement of mass.

If the above-cutoff atoms are treated explicitly, e.g. with a Hartree-Fock approximation [58, 94–96], the need for a high cutoff will be lessened in equilibrium because the above-cutoff HF atoms can successfully take on the kinetic energy. However, when the system is nonstationary, not all is well in that picture because the (possibly dominant) above-cutoff part of the cloud incorrectly remains static, leading to known and feared problems, e.g. with collective excitations [86].

Thus, for strongly nonstationary dynamics, our results indicate that the best looking option is still c-fields but with a high cutoff that can hopefully include dynamics. The small values of  $\text{minRMS}$  found here suggest that such a description can remain correct in the whole regime shown in Fig. 2 *despite* the surprisingly high cutoff.

Support for a high energy cutoff can also be “precoveted”<sup>2</sup> from the well known struggles to describe the thermal dependence of collective frequencies with classical fields. Experiment determined that there is a rather rapid increase in the frequency of the  $m = 0$  quadrupole mode in a 3d trapped system from  $1.85\omega_\perp$  below  $T \approx 0.7T_c$

to  $2\omega_\perp$  above [97]. This has been fairly well matched by ZNG theory [98] and the second-order Bogoliubov of Morgan et al.[99]. In contrast, c-field calculations did not predict a rise in frequency at all ([86]) or only at a temperature that was noticeably too high ( $0.8T_c$ ) [28]. The discrepancy between c-fields and experiment is attributed to a lack of evolution of the above-cutoff part [86].

Interestingly, though, in [86] the dependence of frequency and other observables on the cutoff was studied in the range  $0.65 \leq N_c \lesssim 1$  at the important temperature of  $0.74T_c$ , and the relevant frequency rose encouragingly up to 1.9 at the highest cutoff with  $N_c = 0.65$  (Fig 13 there). 65% of the atoms were then in the c-field. The cutoff increase was not taken further there due to anxiety over including poorly described modes with small occupation. Later, [28] used an even higher energy cutoff ( $N_c = 0.46$ ) and found further improved agreement with experiment. Based on the cutoff dependence of observables presented here, we tentatively conjecture that even further improvement in frequency would be possible with an even higher cutoff that incorporates the majority of high-energy atoms into the c-field, while no major detrimental effect would occur for condensate fraction. Indeed, an almost complete lack of variation in condensate fraction was already shown in Fig 12 of [86], at least for the range of cutoffs studied.

#### D. Nonuniform density

We have seen in Sec. IV A that  $\text{opt } f_c$  is essentially constant in the range of parameters for which thermal fluctuations dominate over quantum ones and matter waves dominate over particle-like behavior. A precursor of this was seen in [69], but Fig. 4 shows the huge scale of it, and how far into the interacting gas it extends.

For a nonuniform gas at a set temperature  $T$ , and interaction  $g$ , we have  $\tau_d = \gamma^2 k_B T / (2\pi g^2)$ . This means that if we consider small sections of the gas in the LDA and move from the densest to less dense parts of the cloud, we are following a straight line in parameter space as shown by the red arrow in Fig. 4. Such lines rise following  $\tau_d \propto \gamma^2$  towards the upper-right. The arrow in the diagram shows the usual experimental situation when  $k_B T \gtrsim \mu$  in the densest region of the gas, so that the starting point is still in the constant cutoff region. All subsequent lower-density sections stay in the  $\text{opt } f_c \approx 0.64$  region until the edge of the classical wave region is reached in the dilute tails of the cloud.

All this means that one cutoff choice is good for the whole cloud when  $k_B T \gtrsim \mu$  — a very convenient result! In more detail, each local piece of the cloud is well described by a local plane-wave basis with the same prescribed  $k_c$  for each such piece. Hence, all the pieces can be described together equally well on a common grid. This also strongly suggests that the whole cloud will be well described whether a plane wave basis or a harmonic oscillator basis is chosen, at least provided the energy

<sup>2</sup> To borrow a term from astronomy.

cutoff used is  $\text{opt}f_c$ . This statement would be also consistent with the typically good agreement seen in numerical studies of trapped gases using these two bases.

The very low temperature case, on the other hand, is more troublesome. Starting lower on the diagram, i.e. with  $k_B T \leq \mu$  ( $\tau_d < \gamma/2\pi$ ), a good description of the system requires a larger  $f_c$  in the center of the cloud than in the tails. This strongly suggests the use of a harmonic oscillator basis which naturally has higher spatial frequencies in the dense centre of the cloud.

If a plane wave basis is used nevertheless for  $k_B T \lesssim \mu$ , then:

- With the high energy cutoff matched to the peak density, the central part of the cloud will be described well. However, the edges and tails will not – as shown in Figs. 3(a) and 1(a). They will have strongly overestimated kinetic energy and excessive  $g^{(2)}(0)$ . Moreover, quantities like phase correlation  $g^{(1)}(z)$ , local  $n_0$ , and density fluctuations  $u_G$  will be underestimated there.
- If one uses the lower cutoff  $\text{opt}f_c \approx 0.64$  that applies for higher temperatures, then the whole outer region with  $k_B T \gtrsim \mu_{\text{eff}}(x) = \mu - V(x)$  will be described well, but the kinetic energy in the center of the cloud will be seriously underestimated. Judging by Fig. 3(c), the remaining macroscopic observables will have only small discrepancies. A bigger problem, though, is that the healing length scale will not be resolved since even the rule-of-thumb cutoff (13) is well above 0.64.

Overall, this analysis suggests the following recommendation for trapped 1d systems: Plane wave or harmonic oscillator bases are equally good while  $k_B T \gtrsim \mu$ , whereas the oscillator basis will become significantly more accurate once temperature drops to  $k_B T < \mu$ .

## VI. COMPARISON OF CUTOFF RESULTS

We present here a mini review of previous cutoff determinations for classical fields in ultracold atoms. Since no comprehensive comparison of these is present in the literature, we have done this here and linked to the present results along the way. As a general overarching comment, the differing sensitivity of the various observables to cutoff that we have described here and in [69] explains how there can be significant differences in cutoff predictions when they are based on single observables, yet no underlying inconsistency.

*a. Early work and arguments for high  $N_c$ .* The earliest c-field works concerned with the dynamics of condensation and phase ordering [3, 24, 36, 60, 100, 101] and the first numerical studies of thermal states [23, 29, 102, 103] were primarily concerned with qualitative aspects. They did not consider the cutoff in any particular detail beyond the fundamental observation that it should occur somewhere between mode occupations of  $N_c \sim \mathcal{O}(10)$  [29]

and  $N_c \ll 1$ . The consensus at this stage was tending to using large values, e.g.  $N_c = 10$  in [102] and  $N_c = 5$  in [79] to keep the c-field approximation (1) accurate for all modes included in  $\mathcal{C}$ . This was re-framed in the more concrete form  $E_c - \mu \ll k_B T$  as a deep, low energy cutoff by [30], while noting that  $N_c \gtrsim 10$  would be excessive [102]. A large number of later works have used  $N_c = 2$  or 3 as their benchmark, which corresponds to  $E_c - \mu \approx (0.3 - 0.5)k_B T$ , i.e.  $\text{opt}f_c \approx (0.3 - 0.4)$  when  $\mu$  is small.

While in hindsight this seems very low compared to (10) here, there are two things to realize: (i) As explained in Sec. V C and seen in Figs. 1 and 3, cutoff choice does not strongly affect the kind of observables usually studied in the early papers, such as condensate fraction in a 3d trapped gas. (ii) It was understood that for quantitative comparison, the above-cutoff atoms would also have to be added, e.g. via a HF approximation. While this was not implemented in the earliest works, the later studies with low energy cutoffs almost always do so, and e.g. [94] confirmed that cutoff dependence of  $n_0$  was then minimal.

*b. Rule of thumb  $E_c \approx k_B T + \mu$ .* Another important but basic observation made early was that in nonuniform interacting systems, the cutoff should obey  $\varepsilon_c \geq \mu$ , in order to properly incorporate the Thomas-Fermi ground state wavefunction [31] and healing-length physics [93]. Later this was refined to  $E_c - E_{\text{ground}} \geq gn_{\text{max}}$  in terms of the maximum density  $n_{\text{max}}$ , and found that  $E_c \gtrsim gn + k_B T \approx \mu + k_B T$  deals sensibly with critical behavior near  $T_c$  [2, 104]. This has become the widely used rule of thumb (13) for interacting systems. One should remember that it is not really consistent with large values of  $N_c$  [22], because it leads to very small  $N_c \propto k_B T / \mu$  in the quantum fluctuation regime ( $\mu \gg k_B T$ ).

*c. Classical effective temperature.* Several early studies noted that the cutoff affects the effective temperature reached at long-time in microcanonical simulations,  $T_{\text{class}}$ . Sinatra *et al.* [37] was the first to study this in the interacting gas in detail, but in the truncated Wigner variant which has special properties. They found  $T_{\text{class}}$  to be strongly affected by the energy converted from initial virtual particles, and along with others [32, 38] argued that one should have much more than 1/2 atom per mode. Consideration of damping rates in the Bogoliubov regime (and the desire to have  $T_{\text{class}}$  not too far from the initial temperature  $T$ ) restricts sensible Wigner cutoffs to energies  $E_c$  of several  $k_B T$  above  $\mu$ . This was a lenient condition compared to the prior postulate  $E_c - \mu \ll k_B T$  of [30], but still indicates  $k_c$  much smaller than the rule of thumb (13) or result (11) found here in the cold Bogoliubov regime of  $k_B T \ll \mu$ . However, it does not clash with the latter results because they are for simple c-fields with no virtual particles.

For these simple c-fields, Schmidt *et al.* [79], and soon after, Davis & Morgan [30], observed that  $T_{\text{class}}$  falls with cutoff because the same energy becomes distributed according to equipartition over more modes. The grand

canonical approach of the SGPE, in contrast, sets the temperature by hand.

*d. Arguments for a low  $N_c$ .* Starting with Brewczyk *et al.*[105], low values of  $N_c$  were explicitly introduced as a compromise between having semi-classicality and trying to describe the whole system without resorting to additional descriptions of above-cutoff atoms. This first paper [105] explicitly assumed  $N_c = 1$ , but later works [25, 106] found even smaller values of  $N_c = 0.6 - 0.7$ . This was found to match condensate fraction  $n_0$  to the ideal gas value in 3d. Although a 40% discrepancy in  $\varepsilon$  arises, there was a conviction at this stage that getting  $n_0$  correct was much more important. A study of damping rates and phase diffusion [107] found that damping rates are generally too small when the cutoff corresponds to Bogoliubov quasiparticle occupations of  $N_c \gtrsim 1$ . There was a suggestion to choose the cutoff at the maximum of the kinetic energy distribution, i.e.  $\varepsilon_c = 1.6k_B T$ , in analogy with Planck's work on the EM field [25]. This also gives  $N_c = 0.6$ . We now know that raising the cutoff even somewhat higher to  $\text{opt}f_c = 0.78$  ( $N_c = 0.52$ ) in the 3d ideal gas [69] satisfies the kinetic energy, without significantly affecting the condensate fraction adversely.

*e. Algorithmic approaches.* A number of algorithmic approaches to determine the cutoff have been proposed, which match c-field results to those obtained from simpler theories. This gives flexibility to deal with different geometries. The aim is generally to get two quantities correct to uniquely specify system parameters. This is similar to single observable-specific cutoffs in our treatment: when  $n$  is matched, one can choose a cutoff that optimizes one further observable  $\Omega$  by setting  $\delta_\Omega(f_c) = 0$ .

- Brewczyk *et al.*[105] worked with c-field ensembles generated with microcanonical time evolution under a given value of  $(gN)$  and cutoff. They used the dual assumptions of  $N_c = 1$  and equipartition in high-energy modes to extract corresponding predictions of  $N$ ,  $g$ , and  $T$ . Their studies lead to one cutoff value that matches the actual values of  $N$ ,  $T$  and  $g$  in a system.
- Zawitkowski *et al.*[106] replaced the  $N_c = 1$  assumption with the more physical condition of matching condensate fraction  $n_0$  between the c-field and the ideal gas. This was adopted for a number of later works in 3d trapped gases and led to  $N_c \approx 0.6 - 0.7$ ,
- Rooney *et al.*[58] first approximated a gas with known  $T$  and  $N$  using a self-consistent combination of a Thomas-Fermi profile for the condensate and quantum Hartree-Fock for excited states. They then chose the cutoff at the Hartree-Fock modes with an occupation of  $N_c = 2$ . This somewhat resembles the  $N_c = 1$  assumption in the approach of [105], but includes above-cutoff atoms in the matching procedure.

- A more robust approach that is applicable to a wider variety of interacting systems was developed by Karpiuk *et al.*[28]. The strategy here is to first approximate the system using a self-consistent Hartree-Fock description with quantum mode occupations that matches known  $T$ ,  $N$ , and condensate fraction  $n_0$  and gives a total field energy  $E_{HF}$ . Then, an initial c-field state with the same energy  $E = E_{HF}$  and  $n_0$  is constructed. The cutoff is then operationally determined as the one that makes the GPE time evolution conserve  $n_0$ . Hence, the match is to HF energy, density, and  $n_0$ . Interestingly, these simulations lead to  $N_c \approx 0.5$ , which agrees very well with the globally optimized 3d ideal gas prescription:  $N_c = 0.52$  [69].

- Cockburn *et al.*[108] first approximated the system using two modified Popov descriptions: one fully quantum and the other with Rayleigh-Jeans mode occupations cut off at  $E_c$ . They then choose the cutoff that matches  $g^{(2)}(0)$  in the center of a 2d trapped cloud. They found that  $g^{(2)}(0)$  is a much more sensitive probe of the cutoff than density  $n$ , and remains sensitive when  $k_B T \lesssim \mu$ . The result is  $E_c \approx 0.78k_B T$ , much lower than the globally optimized cutoff in the 2d ideal gas [69] or the trapped ideal gas value of [27]. Along with the anomalously large  $\text{minRMS}$  in the 2d ideal gas [69], this is an indication that (unlike in 1d and 3d) the cutoffs for the 2d ideal gas are not a good guide for the quasicondensate.

*f. Matching the condensate distribution.* Witkowska *et al.*[27] made an influential study which determined the cutoff that allows one to best match the entire distribution  $P(n_{\text{ex}})$  of the excited fraction in an ideal gas below  $T_c$ . In the canonical ensemble, this is also equivalent to matching the distribution of the condensate fraction,  $P(n_0)$ . They find  $E_c/k_B T = 1, 1.64, 2.19$  in a 1d, 2d, and 3d trap, respectively, corresponding to  $N_c = 1$  or less. Much lower values  $\varepsilon_c/k_B T = 0.29, 0.68, 1.34$  were found for 1-3d uniform boxes, which led to quite large  $N_c$ , even  $N_c = 3.4$  in 1d. The 1d result assumed a system with large condensate fraction and  $L \ll L_\phi$ . As has been noted in [69], there is a fair match between the trapped values and the globally optimal cutoff ( $\varepsilon_c/k_B T = \pi \text{opt}f_c^2 = 1.33, 1.29$ , and 1.91). The results on  $\delta_{n_0}(f_c)$  in Figs. 1 and 3 and in [69] indicate that the remaining difference does not strongly affect  $n_0$  (nor presumably  $P(n_0)$ ), explaining how they coexist. The uniform box results, however, differ a lot from  $\text{opt}f_c$  because they are not in the thermodynamic limit and it is a special system in which canonical and grand canonical ensembles are strongly non-equivalent [109–113].

These results have been used in many later works, often with the “rule of thumb” amendment, i.e. shifting  $\varepsilon_c$  by  $+\mu$  from the ideal gas prescription[91], or shifting down for attractive gases [114]. It was also noted that con-

densate fraction fluctuations  $dn_0/n_0$  are well matched as expected [114], but  $g^{(2)}(0)$  experiences discrepancies (up to  $\approx 10\%$ ) using the above cutoffs [91]. This echoes the greater sensitivity noted by [108]. Bradley *et al.* [42, 115] also found that changing  $E_c$  by 20% introduced only a few percent difference in  $n_0$ .

*g. Other studies.* Calculations of collective frequencies in a 3d trap showed a strong cutoff dependence for the  $m = 0$  quadrupole mode [28, 86] that was similar to the one for  $\varepsilon$ . It appears to be due to the strong dependence on high-energy atoms as explained in Sec. V C. Further, there was no appreciable dependence for the  $m = 2$  mode. The correct treatment likely requires higher  $E_c$  and lower  $N_c$  than in those studies.

It has been noted that when the above-cutoff atoms are treated explicitly, e.g. with a Hartree-Fock approximation, the cutoff dependence of most other quantities becomes small [86, 96]. However, more complicated behavior and cutoff dependence is seen in low dimensional traps that are near the low-d/3d transition when only a few transverse states are important [116].

Bradley *et al.* [117] studied the accuracy of the spectrum and density profile of trapped gases and compared plane wave and harmonic oscillator bases. For plane waves, they found that it is important to have a balance of resolution in both  $x$  and  $k$  space.

Blakie and Davis [118] looked in some detail at the low-energy subspace  $\mathcal{C}$  in 3d trapped gases by counting modes with  $N_c \geq 3$ , a number that correlates with  $E_c$ . It was found that in the ideal gas  $E_c$  is highest at the critical temperature, while for the interacting case it is higher overall but peaks below  $T_c$ . Moreover, a linear growth  $E_c \propto T/T_c$  was seen below  $T_c$  and a sharp drop-off above. This is qualitatively similar to the behavior of  $\varepsilon_c(\text{opt}f_c)$  in [69]. The temperature dependence abated for  $T \ll T_c$ , presumably because of the microcanonical ensemble used.

For the interesting and tricky 2d uniform case, Sato *et al.* [119] compared PGPE values of  $g^{(1)}(z)$  to Monte Carlo studies also with the aim of finding a “well-described region”. They found good agreement and less than 10% variation in  $g^{(1)}(z)$  over a range of cutoffs, with the optimum cutoff for  $g^{(1)}$  growing with temperature: a trend also seen in [69].

## VII. WRAP-UP

By about 2008-2010 the community had come to a general understanding of the considerations for applying c-fields to ultracold bosons, and heuristic approaches for cutoff estimation had been developed. The topic was considered tamed on a qualitative level for the standard observables in equilibrium, but quantitative accuracy and dynamics was considered somewhat suspect unless supported by detailed comparison to experiment. Now, we believe the results obtained here and in [69] provide a broader understanding of the situation and can take the

method to a more precise level than seen before.

We have determined the region of parameter space of the 1d contact-interacting Bose gas where classical-like matter wave physics applies, as shown in Fig. 2. We conclude then that quantitatively accurate studies can be confidently carried out with the classical field approach provided the system stays in this region.

All in all, the region dominated by classical wave physics is larger than one could have conservatively supposed. The entire quasicondensate regime is described well when it comes to the macroscopic observables we have considered, for the whole range of temperatures. This holds even in the colder quantum-depletion-dominated regime of  $k_B T \ll \mu$  down to  $T = 0$ , which was not obvious *a priori*. The great majority of the decoherent regime is correctly described as well, including the quantum turbulent and soliton-dominated regimes [9, 89]. Interestingly, this also means that the changeover from wave-like to particle-like physics occurs at much higher temperatures than the  $\mu = 0$  crossover from the quasicondensate to the HF regime. For 10% error in standard observables, the limits lie at  $\gamma = 0.018$  and  $\tau_d = 0.008$  (i.e.  $\tau = 0.1$  in the notation of [74]), with an additional wedge of classical wave physics extending somewhat beyond these.

The study has also provided information on the appropriate cutoff choice to capture the behavior of many observables in the system simultaneously and obtain the correct energy. It is shown in Fig. 4. The optimal nature of this cutoff stems from the fact that observables have two classes of dependence on cutoff: rising or falling. Hence, the optimum  $\text{opt}f_c$  occurs at a point where there is a balance between rising and falling predictions. The goodness of the description depends on how large the actual discrepancies at this point are.

There are two main regimes regarding cutoff choice. First for  $k_B T \gtrsim \mu$ , when the fluctuations are thermally dominated,  $\text{opt}f_c$  is  $\approx 0.64$  as in (10) and does not depend significantly on any other parameter provided one is in this regime. In the second regime, at very low temperatures  $k_B T \lesssim \mu$  one has (11), with  $\text{opt}f_c \approx \frac{1}{3\sqrt{2\pi}}(\mu/k_B T)^{3/2}$  growing quite rapidly, giving a low cutoff occupation  $N_c \approx 18(\frac{k_B T}{\mu})^3$ . This is needed to correctly capture kinetic energy held in quantum fluctuations. The additional high energy modes have negligible occupation in this regime, so do not appreciably affect other observables. The constant behavior of the optimal cutoff above  $k_B T \gtrsim \mu$  (apart from the standard temperature scaling) across the whole swath of parameter space is a welcome result. It justifies the use of a single cutoff for plane-wave modes even for inhomogeneous gases, provided the high density core does not go into  $\mu \approx gn \gtrsim k_B T$ . If it does, a harmonic oscillator basis becomes strongly recommended.

The globally optimal cutoff that we obtain is noticeably higher than most prior determinations. Remarkably though, it is a result that remains consistent with basically all earlier determinations, as discussed in detail in

Sec. VI. The key to how this can be lies in the fact that some observables such as e.g. condensate fraction depend only very weakly on the cutoff, while others such as kinetic energy are much more sensitive, as seen in Figs. 1 and 3. Since  $\text{minRMS}$  remains small, the various discrepancies  $\delta_\Omega$  remain small as well. This also explains how to reconcile the zoo of earlier cutoff predictions. However, we should keep in mind that we are considering the pure c-field description. An overall cutoff dependence is likely to be both weaker, and different when the above-cutoff modes are approximated using e.g. a Hartree-Fock description — a matter for future study.

An important observation is that the energy per particle (especially kinetic energy) remains the most sensitive criterion for a correct overall description in the interacting gas. This is especially relevant for dynamics where errors in energy feed through into errors in dynamics. Thus, for strongly non-stationary dynamics, the best looking current option are c-fields with a high cutoff that does not underestimate energy density but can include dynamics in quite low occupied modes. The very broad regime of small  $\text{minRMS}$  and constant  $\text{optf}_c$  found here indicates

that such a description can remain robust in 1d *despite* a high-looking cutoff.

Finally, the approach used here to characterize observables and globally optimum behavior could also be helpful in pinpointing the classical wave region and cutoff in other systems such as 2d, 3d, attractive, or multicomponent gases. In particular, the 2d quasicondensate and 3d condensate should be quite readily amenable, as a close-to-exact Bogoliubov description is available for the uniform case [87]. The high-temperature limit should also be accessible with Hartree-Fock methods like those used in [90].

## ACKNOWLEDGMENTS

We are grateful to Mariusz Gajda, Matthew Davis, Blair Blakie, and Nick Proukakis for helpful discussions, and Isabelle Bouchoule for discussions and insight into her experiment. This work was supported by the National Science Centre grant No. 2012/07/E/ST2/01389.

---

[1] M. J. Davis, T. M. Wright, P. B. Blakie, A. S. Bradley, R. J. Ballagh, and C. W. Gardiner, “C-field methods for non-equilibrium bose gases,” in *Quantum Gases* (Imperial College Press, 2013) Chap. 10, pp. 163–175.

[2] P. Blakie, A. Bradley, M. Davis, R. Ballagh, and C. Gardiner, *Advances in Physics* **57**, 363 (2008).

[3] Y. Kagan and B. V. Svistunov, *Phys. Rev. Lett.* **79**, 3331 (1997).

[4] L. E. Sadler, J. M. Higbie, S. R. Leslie, M. Vengalattore, and D. M. Stamper-Kurn, *Nature* **443**, 312 (2006).

[5] C. N. Weiler, T. W. Neely, D. R. Scherer, A. S. Bradley, M. J. Davis, and B. P. Anderson, *Nature* **455**, 948 (2008).

[6] A. D. Martin and J. Ruostekoski, *New Journal of Physics* **12**, 055018 (2010).

[7] E. Witkowska, P. Deuar, M. Gajda, and K. Rzążewski, *Phys. Rev. Lett.* **106**, 135301 (2011).

[8] J. Sabbatini, W. H. Zurek, and M. J. Davis, *New Journal of Physics* **14**, 095030 (2012).

[9] T. Karpiuk, P. Deuar, P. Bienias, E. Witkowska, K. Pawłowski, M. Gajda, K. Rzążewski, and M. Brewczyk, *Phys. Rev. Lett.* **109**, 205302 (2012).

[10] M. Gring, M. Kuhnert, T. Langen, T. Kitagawa, B. Rauer, M. Schreitl, I. Mazets, D. A. Smith, E. Demler, and J. Schmiedmayer, *Science* **337**, 1318 (2012).

[11] C. V. Parker, L.-C. Ha, and C. Chin, *Nature Physics* **9**, 769 (2013).

[12] S. Donadello, S. Serafini, M. Tylutki, L. P. Pitaevskii, F. Dalfovo, G. Lamporesi, and G. Ferrari, *Phys. Rev. Lett.* **113**, 065302 (2014).

[13] S. Serafini, M. Barbiero, M. Debortoli, S. Donadello, F. Larcher, F. Dalfovo, G. Lamporesi, and G. Ferrari, *Phys. Rev. Lett.* **115**, 170402 (2015).

[14] N. Navon, A. L. Gaunt, R. P. Smith, and Z. Hadzibabic, *Science* **347**, 167 (2015).

[15] I.-K. Liu, R. W. Pattinson, T. P. Billam, S. A. Gardiner, S. L. Cornish, T.-M. Huang, W.-W. Lin, S.-C. Gou, N. G. Parker, and N. P. Proukakis, *Phys. Rev. A* **93**, 023628 (2016).

[16] M. C. Tsatsos, P. E. Tavares, A. Cidrim, A. R. Fritsch, M. A. Caracanhas, F. E. A. dos Santos, C. F. Barenghi, and V. S. Bagnato, *Physics Reports* **622**, 1 (2016), quantum turbulence in trapped atomic Bose–Einstein condensates.

[17] R. A. Duine and H. T. C. Stoof, *Phys. Rev. A* **65**, 013603 (2001).

[18] R. J. Lewis-Swan, M. K. Olsen, and K. V. Kheruntsyan, *Phys. Rev. A* **94**, 033814 (2016).

[19] S. P. Cockburn and N. P. Proukakis, “The stochastic gross–pitaevskii methodology,” in *Quantum Gases* (Imperial College Press, 2013) Chap. 11, pp. 177–189.

[20] J. Javanainen and J. Ruostekoski, *New Journal of Physics* **15**, 013005 (2013).

[21] M. D. Lee and J. Ruostekoski, *Phys. Rev. A* **90**, 023628 (2014).

[22] T. M. Wright, M. J. Davis, and N. P. Proukakis, “Reconciling the classical-field method with the beliaev broken-symmetry approach,” in *Quantum Gases* (Imperial College Press, 2013) Chap. 19, pp. 299–312.

[23] K. Góral, M. Gajda, and K. Rzążewski, *Opt. Express* **8**, 92 (2001).

[24] N. G. Berloff and B. V. Svistunov, *Phys. Rev. A* **66**, 013603 (2002).

[25] M. Brewczyk, M. Gajda, and K. Rzążewski, *Journal of Physics B: Atomic, Molecular and Optical Physics* **4**

[26] M. Brewczyk, M. Gajda, and K. Rzążewski, “A classical-field approach for bose gases,” in *Quantum Gases* (Imperial College Press, 2013) Chap. 12, pp. 191–202.

[27] E. Witkowska, M. Gajda, and K. Rzążewski, Phys. Rev. A **79**, 033631 (2009).

[28] T. Karpiuk, M. Brewczyk, M. Gajda, and K. Rzążewski, Phys. Rev. A **81**, 013629 (2010).

[29] M. J. Davis, S. A. Morgan, and K. Burnett, Phys. Rev. Lett. **87**, 160402 (2001).

[30] M. J. Davis and S. A. Morgan, Phys. Rev. A **68**, 053615 (2003).

[31] H. Stoof, Journal of Low Temperature Physics **114**, 11 (1999).

[32] C. W. Gardiner, J. R. Anglin, and T. I. A. Fudge, Journal of Physics B: Atomic, Molecular and Optical Physics **32**, 203002 (2000).

[33] N. P. Proukakis and B. Jackson, Journal of Physics B: Atomic, Molecular and Optical Physics **32**, M555 (2000).

[34] C. W. Gardiner and M. J. Davis, Journal of Physics B: Atomic, Molecular and Optical Physics **32**, S473 (2000).

[35] A. S. Bradley and P. B. Blakie, Phys. Rev. A **90**, 023631 (2014).

[36] M. J. Steel, M. K. Olsen, L. I. Plimak, P. D. Drummond, S. M. Tan, M. J. Collett, D. F. Walls, and R. Graham, Phys. Rev. A **58**, 4824 (1998).

[37] A. Sinatra, C. Lobo, and Y. Castin, Journal of Physics B: Atomic, Molecular and Optical Physics **32**, 1790 (2000).

[38] A. A. Norrie, R. J. Ballagh, and C. W. Gardiner, Phys. Rev. A **73**, 043617 (2006).

[39] A. Polkovnikov, Annals of Physics **325**, 1790 (2010).

[40] J. Ruostekoski and A. D. Martin, “The truncated wigner method for bose gases,” in *Quantum Gases* (Imperial College Press, 2013) Chap. 13, pp. 203–214.

[41] C. Lobo, A. Sinatra, and Y. Castin, Phys. Rev. Lett. **92**, 020403 (2004).

[42] A. S. Bradley, C. W. Gardiner, and M. J. Davis, Phys. Rev. A **77**, 033616 (2008).

[43] R. N. Bisset, M. J. Davis, T. P. Simula, and P. B. Blakie, Phys. Rev. A **79**, 033626 (2009).

[44] B. Damski and W. H. Zurek, Phys. Rev. Lett. **104**, 160404 (2010).

[45] T. Simula, M. J. Davis, and K. Helmerson, Phys. Rev. Lett. **113**, 165302 (2014).

[46] E. Witkowska, T. Świślocki, and M. Matuszewski, Phys. Rev. A **90**, 033604 (2014).

[47] N. G. Parker and C. S. Adams, Phys. Rev. Lett. **95**, 145301 (2005).

[48] T. M. Wright, R. J. Ballagh, A. S. Bradley, P. B. Blakie, and C. W. Gardiner, Phys. Rev. A **78**, 063601 (2008).

[49] J. Sabbatini, W. H. Zurek, and M. J. Davis, Phys. Rev. Lett. **107**, 230402 (2011).

[50] T. Świślocki, E. Witkowska, J. Dziarmaga, and M. Matuszewski, Phys. Rev. Lett. **110**, 045303 (2013).

[51] E. Witkowska, J. Dziarmaga, T. Świślocki, and M. Matuszewski, Phys. Rev. B **88**, 054508 (2013).

[52] M. Anquez, B. A. Robbins, H. M. Bharath, M. Boguslawski, T. M. Hoang, and M. S. Chapman, Phys. Rev. Lett. **116**, 155301 (2016).

[53] B. Nowak, J. Schole, D. Sexty, and T. Gasenzer, Phys. Rev. A **85**, 043627 (2012).

[54] M. Schmidt, S. Erne, B. Nowak, D. Sexty, and T. Gasenzer, New Journal of Physics **14**, 075005 (2012).

[55] M. Karl, B. Nowak, and T. Gasenzer, Phys. Rev. A **88**, 063615 (2013).

[56] B. Nowak, J. Schole, and T. Gasenzer, New Journal of Physics **16**, 093052 (2014).

[57] T. Karpiuk, M. Brewczyk, M. Gajda, and K. Rzążewski, Journal of Physics B: Atomic, Molecular and Optical Physics **42**, 165302 (2009).

[58] S. J. Rooney, A. S. Bradley, and P. B. Blakie, Phys. Rev. A **81**, 023630 (2010).

[59] R. N. Bisset and P. B. Blakie, Phys. Rev. A **80**, 035602 (2009).

[60] R. J. Marshall, G. H. C. New, K. Burnett, and S. Choi, Phys. Rev. A **59**, 2085 (1999).

[61] N. P. Proukakis, J. Schmiedmayer, and H. T. C. Stoof, Phys. Rev. A **73**, 053603 (2006).

[62] M. Wouters and V. Savona, Phys. Rev. B **79**, 165302 (2009).

[63] A. Carusotto, Phys. Rev. A **90**, 023633 (2014).

[64] S. Ayik, Physics Letters B **658**, 174 (2008).

[65] D. Lacroix, D. Gambacurta, and S. Ayik, Phys. Rev. C **87**, 061302 (2013).

[66] S. Klimin, J. Tempere, and J. Devreese, Physica C: Superconductivity and its Applications **503**, 136 (2012).

[67] S. N. Klimin, J. Tempere, G. Lombardi, and J. T. Devreese, EPL **105**, 10002 (2014).

[68] G. D. Moore and N. Turok, Phys. Rev. D **55**, 6538 (1997).

[69] J. Pietraszewicz and P. Deuar, Phys. Rev. A **92**, 063620 (2015).

[70] See supplementary material.

[71] E. H. Lieb and W. Liniger, Phys. Rev. **130**, 1605 (1963).

[72] E. H. Lieb, Phys. Rev. **130**, 1616 (1963).

[73] C. N. Yang and C. P. Yang, Journal of Mathematical Physics **10**, 1115 (1969).

[74] K. V. Kheruntsyan, D. M. Gangardt, P. D. Drummond, and G. V. Shlyapnikov, Phys. Rev. Lett. **91**, 040403 (2003).

[75] K. V. Kheruntsyan, D. M. Gangardt, P. D. Drummond, and G. V. Shlyapnikov, Phys. Rev. A **71**, 053615 (2005).

[76] A. G. Sykes, D. M. Gangardt, M. J. Davis, K. Viering, M. G. Raizen, and K. V. Kheruntsyan, Phys. Rev. Lett. **100**, 160406 (2008).

[77] P. Deuar, A. G. Sykes, D. M. Gangardt, M. J. Davis, P. D. Drummond, and K. V. Kheruntsyan, Phys. Rev. A **79**, 043619 (2009).

[78] E. Witkowska, M. Gajda, and K. Rzążewski, Optics Communications **283**, 671 (2010).

[79] H. Schmidt, K. Góral, F. Floegel, M. Gajda, and K. Rzążewski, Journal of Optics B: Quantum and Semiclassical Optics **5**, S96 (2003).

[80] J. Esteve, J.-B. Trebbia, T. Schumm, A. Aspect, C. I. Westbrook, and I. Bouchoule, Phys. Rev. Lett. **96**, 130403 (2006).

[81] C. Sanner, E. J. Su, A. Keshet, R. Gommers, Y.-i. Shin, W. Huang, and W. Ketterle, Phys. Rev. Lett. **105**, 040402 (2010).

[82] T. Müller, B. Zimmermann, J. Meineke, J.-P. Brantut, T. Esslinger, and H. Moritz, Phys. Rev. Lett. **105**, 040401 (2010).

[83] T. Jacqmin, J. Armijo, T. Berrada, K. V. Kheruntsyan, and I. Bouchoule, Phys. Rev. Lett. **106**, 230405 (2011).

[84] J. Armijo, T. Jacqmin, K. Kheruntsyan, and I. Bouchoule, Phys. Rev. A **83**, 021605 (2011).

[85] J. Armijo, Phys. Rev. Lett. **108**, 225306 (2012).

[86] A. Bezett and P. B. Blakie, Phys. Rev. A **79**, 023602 (2009).

[87] C. Mora and Y. Castin, Phys. Rev. A **67**, 053615 (2003).

[88] J. Pietraszewicz and P. Deuar, “The statistics of density grains in the 1d interacting bose gas from the yang-yang exact solution,” (2017), in preparation.

[89] I. Nowicki, J. Pietraszewicz, and P. Deuar, “The soliton regime in ultracold bose gases,” (2017), in preparation.

[90] C. Henkel, T.-O. Sauer, and N. P. Proukakis, arXiv:1701.03133 (2017).

[91] P. Bienias, K. Pawłowski, M. Gajda, and K. Rzążewski, Phys. Rev. A **83**, 033610 (2011).

[92] V. A. Kashurnikov, N. V. Prokof'ev, and B. V. Svistunov, Phys. Rev. Lett. **87**, 120402 (2001).

[93] Y. Castin, J. Phys. IV France **116**, 89 (2004).

[94] M. J. Davis and P. B. Blakie, Phys. Rev. Lett. **96**, 060404 (2006).

[95] S. P. Cockburn, D. Gallucci, and N. P. Proukakis, Phys. Rev. A **84**, 023613 (2011).

[96] S. P. Cockburn, A. Negretti, N. P. Proukakis, and C. Henkel, Phys. Rev. A **83**, 043619 (2011).

[97] D. S. Jin, M. R. Matthews, J. R. Ensher, C. E. Wieman, and E. A. Cornell, Phys. Rev. Lett. **78**, 764 (1997).

[98] B. Jackson and E. Zaremba, Phys. Rev. Lett. **88**, 180402 (2002).

[99] S. A. Morgan, M. Rusch, D. A. W. Hutchinson, and K. Burnett, Phys. Rev. Lett. **91**, 250403 (2003).

[100] K. Damle, S. N. Majumdar, and S. Sachdev, Phys. Rev. A **54**, 5037 (1996).

[101] P. D. Drummond and J. F. Corney, Phys. Rev. A **60**, R2661 (1999).

[102] M. J. Davis, R. J. Ballagh, and K. Burnett, Journal of Physics B: Atomic, Molecular and Optical Physics **34**, 4487 (2001).

[103] M. J. Davis, S. A. Morgan, and K. Burnett, Phys. Rev. A **66**, 053618 (2002).

[104] A. Bezett and P. B. Blakie, Phys. Rev. A **79**, 033611 (2009).

[105] M. Brewczyk, P. Borowski, M. Gajda, and K. Rzążewski, Journal of Physics B: Atomic, Molecular and Optical Physics **37**, 2725 (2004).

[106] L. Zawitkowski, M. Brewczyk, M. Gajda, and K. Rzążewski, Phys. Rev. A **70**, 033614 (2004).

[107] A. Sinatra and Y. Castin, Phys. Rev. A **78**, 053615 (2008).

[108] S. P. Cockburn and N. P. Proukakis, Phys. Rev. A **86**, 033610 (2012).

[109] H. D. Politzer, Phys. Rev. A **54**, 5048 (1996).

[110] P. Navez, D. Bitouk, M. Gajda, Z. Idziaszek, and K. Rzążewski, Phys. Rev. Lett. **79**, 1789 (1997).

[111] C. Weiss and M. Wilkens, Opt. Express **1**, 272 (1997).

[112] V. V. Kocharovsky, V. V. Kocharovsky, M. Holthaus, C. R. Ooi, A. Svidzinsky, W. Ketterle, and M. O. Scully, Advances In Atomic, Molecular, and Optical Physics **53**, 291 (2006).

[113] J. Pietraszewicz, E. Witkowska, and P. Deuar, arXiv:1706.02587 (2017).

[114] P. Bienias, K. Pawłowski, M. Gajda, and K. Rzążewski, EPL (Europhysics Letters) **96**, 10011 (2011).

[115] A. S. Bradley and C. W. Gardiner, arXiv:cond-mat/0602162 (2006).

[116] A. S. Bradley, S. J. Rooney, and R. G. McDonald, Phys. Rev. A **92**, 033631 (2015).

[117] A. S. Bradley, P. B. Blakie, and C. W. Gardiner, Journal of Physics B: Atomic, Molecular and Optical Physics **38**, 4259 (2005).

[118] P. B. Blakie and M. J. Davis, Journal of Physics B: Atomic, Molecular and Optical Physics **44**, 035001 (2011).

[119] T. Sato, Y. Kato, T. Suzuki, and N. Kawashima, Phys. Rev. E **85**, 050105 (2012).

### Supplementary material for:

## Complex wave fields in the interacting 1d Bose gas: when do they apply, and where to cut off the coherent region?

J. Pietraszewicz and P. Deuar

*Institute of Physics, Polish Academy of Sciences, Al. Lotników 32/46, 02-668 Warsaw, Poland*

We describe here the more technical elements of the paper, including some raw data and methods employed. Citation numbers refer to the bibliography in the main paper.

### S1. NUMERICAL CLASSICAL FIELD ENSEMBLES

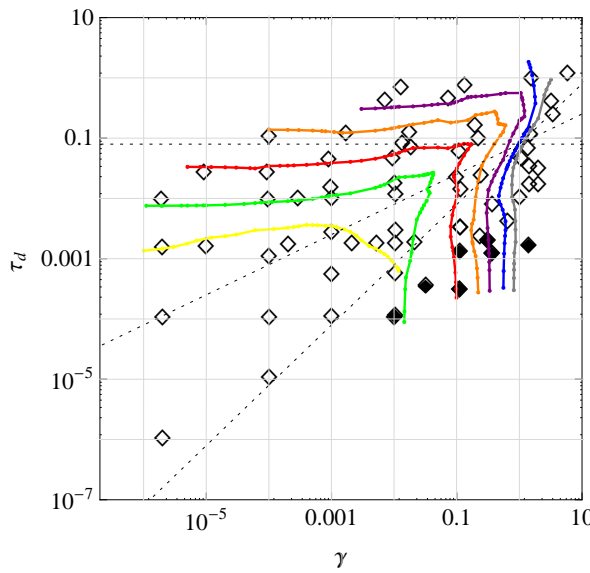


Figure S1. This diagram shows the location of numerical ensembles that were used to produce Figs. 2, 4 and S4. Metropolis and SGPE ensembles are shown as open and filled diamonds, respectively. Contours of  $\text{minRMS}$  at values of 0.05, 0.1, 0.2, 0.3, 0.4, 0.5, and 0.6 are shown for context.

In this section we explain some details of the classical field ensembles that were obtained numerically.

#### A. Overview

For each of the pairs of parameters  $\gamma, \tau_d$  shown in Fig. S1, about 10-15 ensembles of  $\Psi(x)$  with different cut-off values  $f_c$  were generated and used to evaluate c-field observables  $\Omega^{(\text{cf})}(\gamma, \tau_d, f_c)$ . The values of  $f_c$  were chosen individually for each  $\gamma, \tau_d$  pair to cover the region of the minimum of  $RMS(f_c)$  with a resolution that is sufficient to determine  $\text{minRMS}$  and  $\text{opt}f_c$  to a satisfactory degree. This was usually 10-20 values, as shown e.g. by the

data points in Figs. 1 and S3. Each ensemble consisted of  $10^3 - 10^4$  members. The members were generated using either a Metropolis algorithm (see Sec. S1B) or a stochastic Gross-Pitaevskii (SGPE) equation simulation (see Sec. S1C). The former are shown as empty symbols in Fig. S1 and the latter as filled symbols. The SGPE was used in the lower temperatures with  $k_B T \ll \mu$ , where it turned out to be more efficient.

The generation of the ensembles is parametrized by the values of  $T, \mu, g$ , and the numerical lattice. This is not immediately convertible to  $\gamma$  and  $\tau_d$ , since these quantities depend on  $n$ , and  $n = \langle N \rangle / L$  depends numerically on the actual ensemble generated. To deal with this inverse problem, we proceeded as follows: First a target pair of  $\gamma^{\text{target}}, \tau_d^{\text{target}}$  is chosen. This gives  $g$  and a target density  $n^{\text{target}}$  from (2). Next, the Yang-Yang exact solution (see Sec. S2) is obtained, giving the value of  $\mu$  that generates the target density in the full quantum description<sup>3</sup>. This is usually close but not exactly equal to a chemical potential  $\mu^{(\text{cf})}(f_c)$  that would give the same density of the c-field ensemble. In any case,  $\mu^{(\text{cf})}$  depends on the chosen  $f_c$ . Nevertheless, since  $\mu$  and  $\mu^{(\text{cf})}$  are close, we simply use the target quantum  $\mu$  and various values of  $f_c$  to generate each ensemble, knowing that it will be close to  $\gamma^{\text{target}}$  and  $\tau_d^{\text{target}}$ .

Each ensemble with a different  $f_c$  generates a slightly different mean particle density  $n^{(\text{cf})}(f_c) = \langle N \rangle / L$ , and corresponding  $\gamma^{(\text{cf})}(f_c), \tau_d^{(\text{cf})}(f_c)$  which lie close to but not exactly at  $\gamma^{\text{target}}, \tau_d^{\text{target}}$ . However, it is not necessary to hit exact predetermined target values for our purpose of generating contour diagrams. Instead, the value of  $n$  at the optimal cutoff  $\text{opt}f_c$  was the one used to determine the operational values of

$$\gamma = \frac{mg}{\hbar^2 n^{(\text{cf})}(\text{opt}f_c)}, \quad \tau_d = \frac{mk_B T}{2\pi\hbar^2 n^{(\text{cf})}(\text{opt}f_c)^2} \quad (\text{S1})$$

used for the analysis (and shown in Fig. S1).

<sup>3</sup> There is one free scaling parameter in the description using  $\gamma$  and  $\tau_d$ , which we set in the Yang-Yang calculations using the arbitrary choice  $k_B T = 1$ .

The numerical lattice itself, is chosen according to the usual criteria to obtain a system in the thermodynamic limit. The box length  $L$  must be sufficient to capture the longest length scales. The longest feature is the width of the  $g^{(1)}(z)$  phase correlation function, and  $L$  was chosen so that  $g^{(1)}$  decays to zero before reaching a distance of  $z = L/2$ . Namely,  $g^{(1)}(L/2)$  found from the ensemble falls closer to zero than its statistical uncertainty. On the other hand, the lattice spacing  $\Delta x$  must be sufficiently small to resolve the smallest allowable features. These are the density ripples of a standing wave composed of waves with the cutoff momentum  $k_c$ . That is we need  $\Delta x \leq \pi/(2k_c)$ . In practice we took a several times finer spacing  $\Delta x$  to smooth the visible features. The numerical lattices contained  $M = 2^{10} - 2^{12}$  points.

Periodic boundary conditions were used, to have easy access to plane wave modes through Fourier transforms. The c-field was given support only within the low-energy subspace  $\mathcal{C}$  by keeping only the  $M_{\mathcal{C}}$  plane wave components of the Fourier transformed field with  $|k| \leq k_c$ .

## B. Metropolis algorithm

Our application of the Metropolis method to generate c-field ensembles follows the approach of Witkowska et al. [78], with minor modifications as used in [69]. The latter paper introduced amendments to generate grand canonical ensembles, primarily by removing the conservation of  $N$  used in [78]. This has the additional advantage of removing the need for a small but tricky compensation that is otherwise needed to preserve detailed balance in the number-conserving case.

We aim to generate the grand canonical probability distribution

$$P(\Psi) \propto \exp \left[ -\frac{E_{\text{kin}}(\Psi) + E_{\text{int}}(\Psi) - \mu N(\Psi)}{k_B T} \right]. \quad (\text{S2})$$

where

$$N(\Psi) = \sum_x \Delta x |\Psi(x)|^2, \quad (\text{S3})$$

and energies are

$$E_{\text{int}}(\Psi) = \frac{g \Delta x}{2} \sum_x |\Psi(x)|^4, \quad (\text{S4})$$

$$E_{\text{kin}}(\Psi) = \frac{\hbar}{2m} \sum_k \Delta k k^2 |\tilde{\Psi}(k)|^2. \quad (\text{S5})$$

The kinetic energy uses the Fourier transformed field normalized to make  $\sum_k \Delta k |\tilde{\Psi}(k)|^2 = N$ , i.e.

$$\tilde{\Psi}(k) = \frac{1}{\sqrt{2\pi}} \sum_x \Delta x e^{-ikx} \Psi(x) \quad (\text{S6})$$

with wavevectors  $k = 2\pi j/L = j\Delta k$ , and  $j$  integers.

The starting state was  $\Psi_0(x) = 0$ .

A random walk is then initiated which generates a Markov chain with members  $\Psi_s(x)$  after each step  $s$ . A trial update  $\Psi^{\text{trial}}(x)$  is generated at each step. The ratio of probabilities

$$r = \frac{P(\Psi^{\text{trial}})}{P(\Psi_s)} \quad (\text{S7})$$

is evaluated. The update is accepted always if  $r > 1$ , or with probability  $r$  if  $0 < r < 1$ . Then the next member of the random walk  $\Psi_{s+1}$  becomes  $\Psi^{\text{trial}}$ . Otherwise the update is rejected, and  $\Psi_{s+1} = \Psi_s$ .

We used two kinds of updates, chosen randomly at each step:

1. 99%/ $M_{\mathcal{C}}$  probability: A change of the amplitude of one of the plane wave modes  $k'$ , such that  $\tilde{\Psi}^{\text{trial}}(k') = \tilde{\Psi}_s(k') + \delta$  while the other modes are unchanged:  $\tilde{\Psi}^{\text{trial}}(k \neq k') = \tilde{\Psi}_s(k)$ . The random shift  $\delta$  is a Gaussian distributed complex random number with amplitude chosen so that the acceptance ratio is about 50%. The value of  $k'$  to change is chosen randomly from the  $M_{\mathcal{C}}$  plane wave modes that lie below the energy cutoff.
2. 1% probability: We found that it is necessary to sometimes slightly shift the center of mass of the system to break the system out of getting stuck on a nonzero mean velocity. For this, one generates  $\tilde{\Psi}^{\text{trial}}(k) = \tilde{\Psi}_s(k \pm \Delta k)$ , shifting all values by one lattice point. The sign is chosen randomly, and the wavefunction  $\Psi(\bar{k})$  at the marginal value of  $\bar{k} = \pm(k_c + \Delta k)$  that overflows  $k_c$  due to the shift is moved to the opposite end of the spectrum at  $\mp(k_c)$ .

Since all of these updates preserve detailed balance individually, no additional compensation to  $r$  is required to determine acceptance, unlike in the  $N$ -conserving algorithm for the canonical ensemble.

The correlation of various quantities such as  $E$ ,  $N$ ,  $g^{(1)}(z)$  and the center-of-mass momentum  $k_{COM}$  over subsequent steps  $s$  is tracked. Ergodicity is then exploited to obtain independent ensemble members by placing only every  $\Delta s$ -th member of the Markov chain into the final ensemble. The spacing  $\Delta s$  is chosen sufficiently large to make all the observables uncorrelated. Also, the first  $t_s \gtrsim \Delta s$  elements of the Markov chain are discarded to allow for the dissipation of transients caused by the starting state. The required  $\Delta s$  and  $t_s$  depend on the regime studied. Generally speaking, when  $\gamma < \tau_d$ , we had  $\Delta s = \mathcal{O}(10^4 - 10^5)$ , while in the opposite regime ( $\gamma > \tau_d$ )  $\Delta s$  was even larger, causing us to switch to using the SPGPE algorithm.

### C. SPGPE algorithm

The projected stochastic Gross-Pitaevskii equation (SPGPE) [34, 35] is here

$$i\hbar \frac{d\Psi(x)}{dt} = (1 - i\gamma_c) \mathcal{P}_c \left\{ \left[ -\frac{\hbar^2}{2m} \frac{d^2}{dx^2} - \mu + g|\Psi(x)|^2 \right] \Psi(x) + \sqrt{2\hbar\gamma_c k_B T} \eta(x, t) \right\} \quad (\text{S8})$$

This approach has been extensively used to generate grand canonical ensembles of  $\Psi(x)$  and described in detail in [17, 19, 33, 34]. The quantity  $\eta(x, t)$  is a complex time-dependent white noise field with the properties

$$\langle \eta(x, t)\eta(x', t') \rangle = \langle \eta(x, t) \rangle = 0 \quad (\text{S9a})$$

$$\langle \eta(x, t)^* \eta(x', t') \rangle = \delta(x - x')\delta(t - t'). \quad (\text{S9b})$$

It is generated using Gaussian random numbers of variance  $1/(\Delta x \Delta t)$  where time steps are  $\Delta t$  and the numerical spatial lattice is  $\Delta x$ . The  $\mathcal{P}_c$  is a projector onto the low-energy subspace. A quantity  $\mathcal{P}_c\{A(x)\}$  is implemented by Fourier transforming  $A(x)$  to k-space, zeroing out all components with  $|k| > k_c$ , and Fourier transforming back again to x-space.

The physical model in the SGPE treats the above-cutoff atoms as a thermal and diffusive bath with temperature  $T$ , chemical potential  $\mu$ , and a coupling strength  $\gamma_c$  between the low- and high-energy subspaces. We typically used  $\gamma_c = 0.02$ . The long-time limit of an ensemble of many such trajectories is the grand canonical ensemble with  $T$  and  $\mu$  the same as the bath. To obtain an ensemble we started with the standard vacuum initial states  $\Psi(x) = 0$  and ran the simulation multiple times, with new noises in each run to generate a new trajectory. Ensemble averaged quantities were tracked over time until all reached stationary values. Then, the fields at this stabilized time were taken as the members of the final ensemble, usually with 400-2000 members.

Apart from faster convergence, this approach requires less numerical tweaking than the Metropolis algorithm since it is unnecessary to search for the correlation time  $\Delta s$  in the Markov chain, while the size of the fluctuations is chosen automatically instead of optimizing  $\delta$  to get reasonable acceptance rates. On the other hand, only the grand canonical ensemble can be generated using (S8). However, a more complicated “scattering term” SPGPE derived by Rooney *et al.*<sup>4</sup> does conserve  $N$ , and a simple modified SPGPE for canonical ensembles has been derived recently [113].

### S2. EXACT QUANTUM RESULTS

To obtain the exact quantum results, we numerically self-consistently solve the integral equations found by Yang and Yang [73]. These give an exact solution for the 1d contact interacting repulsive Bose gas in the thermodynamic limit. The input parameters are  $\mu_Q$ ,  $T$ , and  $g$ , and this directly allows one to calculate the mean number of particles  $N$ , energy  $E$ , entropy  $S$ , and pressure  $P$  as described in [73]. To obtain results for a given  $\gamma$  and  $\tau_d$ , one needs to have results for a set density  $n$ . For this, the relation  $n(\mu_Q, T, g)$  has to be inverted. We do this numerically, using trial input  $\mu_Q$  values, and iterative interpolation until the matching  $n$  is obtained.

The Hellmann-Feynmann theorem has been used [74] to obtain an expression for  $g^{(2)}(0)$ . We use the more convenient version from [75]:

$$g^{(2)}(0) = -\frac{1}{n^2} \left( \frac{\partial P}{\partial g} \right)_{\mu_Q, T}. \quad (\text{S10})$$

To evaluate the derivative, we obtain three sets of results for the same  $\mu_Q$  and  $T$ , but with  $g$ ,  $g \pm \Delta g/2$ . Then we can approximate

$$g^{(2)}(0) \approx -\frac{1}{n(g)^2} \frac{P(g + \frac{1}{2}\Delta g) - P(g - \frac{1}{2}\Delta g)}{\Delta g}. \quad (\text{S11})$$

$\Delta g = 0.0001g$  was used. The kinetic energy can then also be readily obtained since  $E/N = \varepsilon + (\frac{gn}{2}) g^{(2)}(0)$ .

The coarse-grained fluctuations can, in turn be obtained from the equation of state using

$$\text{var}N = Nu_G = k_B T \left( \frac{\partial N}{\partial \mu_Q} \right)_{g, T} \quad (\text{S12})$$

as explained by Armijo *et al.*<sup>5</sup>. This can also be evaluated in principle with a numerical derivative similar to (S11), but it turns out to be inconveniently sensitive to numerical details. Instead we developed a computational refinement described in [88] that uses a new set of integral equations:

In the Yang-Yang theory,  $N$  is given by an integral

$$N = L \int_{-\infty}^{\infty} \rho(k) dk \quad (\text{S13})$$

of the (dimensionless) density of occupied quasimomenta  $\rho(k)$ . The  $\rho(k)$  along with a spectrum  $\epsilon(k)$  are given as the solution of a pair of coupled integral equations dependent on  $\mu_Q$  (called  $A$  in [73]),  $T$ , and  $g$  (called  $2c$  in [73]).<sup>6</sup>

<sup>5</sup> J. Armijo, T. Jacqmin, K. V. Kheruntsyan, and I. Bouhoule, Phys. Rev. Lett. **105**, 230402 (2010).

<sup>6</sup> Note that on top of this renaming of  $\mu_Q = A$  and  $g = 2c$ , [73] uses  $\hbar = k_B = 2m = 1$  units that introduce another somewhat confusing factor of 2. We refer the reader to [88] for clarification.

<sup>4</sup> S. J. Rooney, P. B. Blakie, and A. S. Bradley, Phys. Rev. A **86**, 053634 (2012).

Since (S12) takes a derivative of (S13) with respect to  $\mu_Q$ , we can also calculate it via

$$u_G = \frac{T}{n} \int_{-\infty}^{\infty} \rho'(k) dk \quad (\text{S14})$$

where

$$\rho'(k) = \frac{\partial \rho(k)}{\partial \mu_Q}. \quad (\text{S15})$$

This is given by the solution of the new integral equation

$$\rho'(k) \left[ 1 + e^{\epsilon(k)/T} \right] + \frac{\rho(k) \epsilon'(k)}{T} e^{\epsilon(k)/T} = \frac{c}{\pi} \int_{-\infty}^{\infty} \frac{dq \rho'(q)}{c^2 + (k - q)^2}. \quad (\text{S16})$$

The above is written in terms of the quantity

$$\epsilon'(k) = \frac{\partial \epsilon(k)}{\partial \mu_Q}, \quad (\text{S17})$$

which, in turn, can be obtained from a second integral equation obtained from differentiating the one for  $\epsilon(k)$  in [73]:

$$\epsilon'(k) = -1 + \frac{c}{\pi} \int_{-\infty}^{\infty} \frac{dq \epsilon'(q)}{c^2 + (k - q)^2} \frac{1}{1 + e^{\epsilon(q)/T}}. \quad (\text{S18})$$

The two integral equations can be solved by iteration starting from a source term with integral discarded, similarly to what was done in [73] for the original quantities  $\epsilon(k)$  and  $\rho(k)$ .

For comparison of c-field and exact quantum values in (6) and (8), we generate matching exact quantum results that have the same density as each particular classical field ensemble or Bogoliubov calculation. That is, for each  $n^{(\text{cf})}(f_c)$  we generate exact quantum results with the same  $T$  and  $g$ , but a matching  $\mu_Q(f_c)$  chosen separately for each ensemble with a different cutoff,  $\gamma$  or  $\tau_d$ . The match is so that  $N(\mu_Q(f_c), T, g)/L = n^{(\text{cf})}(f_c)$ .

### 3. BOGOLIUBOV CALCULATIONS

For the lowest temperatures, and particularly in the dilute limit, both SGPE and exact Yang-Yang calculations become very inefficient. The former converge very slowly to the true equilibrium distribution, while the latter require ever larger numerical lattices to accurately solve the required integral equations. Fortunately, this is the quasicondensate regime in which the extended Bogoliubov theory of Mora & Castin becomes very accurate [87]. This extension of the standard Bogoliubov description relaxes the small condensate depletion condition, and only requires that the *density fluctuations* are small. It allows for the description of quasicondensates with  $N_0/N \rightarrow 0$ .

We have used this extended Bogoliubov theory in the parameter regimes that are difficult to access using numerical ensembles and Yang-Yang. The quantum Bogoliubov description is used in lieu of the Yang-Yang calculations to generate quantum observables  $\Omega^{(\text{q})} \rightarrow \Omega^{(\text{Bog-q})}$

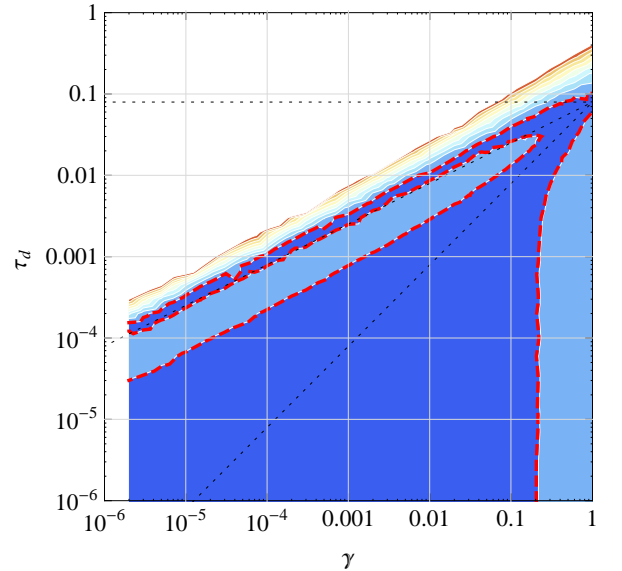


Figure S2. This diagram shows the region (dark blue) where the Bogoliubov treatment is accurate by plotting contours (at 0.1, 0.2, ..., 1.0) of the discrepancy (S19) between the quantum Bogoliubov treatment and exact Yang-Yang theory. The  $RMS^{(Q)} = 0.1$  contour is shown as a thick red dashed line.

in (6). A c-field equivalent is used in lieu of the numerical ensembles to generate the observable estimates  $\Omega^{(\text{cf})}(f_c) \rightarrow \Omega^{(\text{Bog-cf})}(f_c)$ . To compare observable predictions here we match the output densities, but not the input chemical potentials.

#### A. Accuracy of the extended Bogoliubov theory

The region in which this approach gives correct results can be seen in Fig. S2, circumscribed by the red dashed line. A figure of merit for the accuracy of the Bogoliubov theory over many observables similar to (8) is

$$RMS^{(Q)}(\gamma, \tau_d) = \sqrt{(\delta_{u_G}^{(\text{Bog})})^2 + \max \left[ (\delta_{\varepsilon}^{(\text{Bog})})^2, (\delta_{\varepsilon_{\text{tot}}}^{(\text{Bog})})^2 \right]}, \quad (\text{S19})$$

where

$$\delta_{\Omega}^{(\text{Bog})}(\gamma, \tau_d) = \left( \frac{\Omega^{(\text{Bog-q})}(\gamma, \tau_d)}{\Omega^{(\text{q})}(\gamma, \tau_d)} - 1 \right). \quad (\text{S20})$$

Again, the region with less than 10% error corresponds to  $RMS^{(Q)} < 0.1$ . We restrict our use of the Bogoliubov theory for generating results in Figs. 2 and 4 to this region, and only to its main contiguous part. That is, we discard the narrow “valley” heading upwards and right of  $\tau_d = 10^{-4}$ ,  $\gamma = 2 \times 10^{-6}$  and the region above  $\tau_d = 0.01$ . Judging by the fact that regions with poor performance of the Bogoliubov theory appear very close nearby, the small values of  $RMS^{(Q)}$  in these narrow areas are probably due to a lucky and fragile match of the observables

entering the formula  $RMS^{(Q)}$ . Other observables may not be so lucky here.

Further evidence of the accuracy of the approach in which both c-fields and quantum results are restricted to Bogoliubov quasiparticles is seen in Fig. S4. There is an excellent match between the contours produced by the Bogoliubov approach and the complete approach, in the region where both are valid (i.e. between the dashed red lines for Bogoliubov, and as far down as the numerical ensemble results reach).

## B. Quantum Bogoliubov for a uniform gas

This is described in complete detail in [87]. Summarizing the uniform 1d case, the quantum field is written as

$$\hat{\Psi}(x) = e^{i\hat{\theta}(x)} \sqrt{\hat{\rho}(x)}, \quad \hat{\rho}(x) = \rho_0(x) + \delta\hat{\rho}(x). \quad (\text{S21})$$

The density estimate from a GPE solution is

$$\rho_0 = \frac{\mu}{g}. \quad (\text{S22})$$

Two small parameters are assumed: density fluctuations  $|\delta\hat{\rho}| \ll \rho_0$  which make this a quasicondensate, and  $|\hat{\theta}(x + \Delta x) - \hat{\theta}(x)| \ll 1$  which amounts to saying that a (fine) discretization of space corresponds to the continuum model. The latter is needed to self-consistently define the operator  $\hat{\theta}$  in (S21). The exact quantum model is then truncated to 2nd or 3rd order in these small parameters as the situation warrants.

The Hamiltonian can be brought to the quasiparticle form

$$\hat{H} = \sum_{k \neq 0} E_k \hat{b}_k^\dagger \hat{b}_k + \frac{g}{2L} \hat{P}^2 + E_{\text{ground}} \quad (\text{S23})$$

where  $\hat{b}_k$  are quasiparticle annihilation operators for all plane wave modes except  $k = 0$ , with the usual commutation relation  $[\hat{b}_k, \hat{b}_{k'}^\dagger] = \delta_{kk'}$ . The quasiparticle energy is

$$E_k = \sqrt{\epsilon_k(\epsilon_k + 2\mu)}, \quad (\text{S24})$$

in terms of the free-particle energy

$$\epsilon_k = \frac{\hbar^2 k^2}{2m} \quad (\text{S25})$$

and  $\mu$ .  $\hat{P}$  is a dimensionless operator related to fluctuations in the total number of particles. There is also a zero energy collective coordinate for the quantum phase of the field,  $\hat{Q}$ . They have the mutual commutation relation  $[\hat{P}, \hat{Q}] = -i$  and commute with all  $\hat{b}$  and  $\hat{b}^\dagger$ .

For the purpose of evaluating observables, the wavefunction elements of (S21) can be expanded as

$$\begin{aligned} \delta\hat{\rho}(x) &= \sqrt{\frac{\rho_0}{L}} \sum_{k \neq 0} (\bar{u}_k + \bar{v}_k) \left[ e^{ikx} \hat{b}_k + e^{-ikx} \hat{b}_k^\dagger \right] + \frac{\hat{P}}{L} \\ \hat{\theta}(x) &= \frac{1}{2i\sqrt{\rho_0 L}} \sum_{k \neq 0} (\bar{u}_k - \bar{v}_k) \left[ e^{ikx} \hat{b}_k - e^{-ikx} \hat{b}_k^\dagger \right] - \hat{Q} \end{aligned} \quad (\text{S26})$$

where the quasiparticle wavefunction amplitudes are

$$\bar{u}_k \pm \bar{v}_k = \left[ \frac{\epsilon_k}{\epsilon_k + 2\mu} \right]^{\pm 1/4}. \quad (\text{S27})$$

In thermal equilibrium all single operators  $\hat{b}$ ,  $\hat{b}^\dagger$ ,  $\hat{P}$  and the anomalous average  $\hat{b}_k \hat{b}_{k'}$  have zero mean, while occupations are  $\langle \hat{b}_k^\dagger \hat{b}_k \rangle = \delta_{kk'} n_k$  with

$$n_k = \frac{1}{e^{E_k/k_B T} - 1}. \quad (\text{S28})$$

Also,  $\langle \hat{P}^2 \rangle = k_B T \frac{L}{g}$ . Averages involving  $\hat{Q}$  are usually unnecessary. In the thermodynamic limit, the sum  $\sum_{k \neq 0}$  can be replaced<sup>7</sup> by  $\frac{L}{2\pi} \int_{-\infty}^{\infty} dk$ .

The equation of state is given by an integral:

$$n = \frac{\mu}{g} - \int_{-\infty}^{\infty} \frac{dk}{2\pi} \left[ (\bar{u}_k + \bar{v}_k)^2 n_k + \bar{v}_k (\bar{u}_k + \bar{v}_k) \right]. \quad (\text{S29})$$

It allows us to retroactively obtain  $\mu/k_B T$  from given values of  $\gamma$  and  $\tau_d$ . This is possible because the latter set  $g$  and  $n$  via (2), apart from one free scaling parameter  $k_B T$ . At  $T = 0$ ,  $\mu = ng(1 - 1/\pi n \xi)$  and the healing length is

$$\xi = \frac{\hbar}{\sqrt{m\mu}}. \quad (\text{S30})$$

Other observables are obtained as follows:

$$g^{(2)}(z) = 1 + \frac{2}{n} \int_{-\infty}^{\infty} \frac{dk}{2\pi} \left[ (\bar{u}_k + \bar{v}_k)^2 n_k + \bar{v}_k (\bar{u}_k + \bar{v}_k) \right] \cos kz. \quad (\text{S31})$$

leading via (7) to the convenient

$$u_G = 1 + 2 \lim_{k \rightarrow 0} \left[ (\bar{u}_k + \bar{v}_k)^2 n_k + \bar{v}_k (\bar{u}_k + \bar{v}_k) \right] = \frac{k_B T}{\mu}. \quad (\text{S32})$$

The interaction energy per particle is trivially related to  $g^{(2)}(0)$  straight from the Hamiltonian:

$$\mathcal{E}_{\text{int}} = \frac{gn}{2} g^{(2)}(0) = \mu - k_B T \frac{\gamma}{4\pi\tau_d}. \quad (\text{S33})$$

<sup>7</sup> This is notwithstanding the fact that the theory in [87] is written in terms of a fine discretization of space with spacing  $\Delta x$ . This formally corresponds to  $\int_{-\pi/\Delta x}^{\pi/\Delta x}$ , but for any well described physical quantity the result must be unchanged in the limit  $\Delta x \rightarrow 0$ .

The final expression comes from identifying the same integrals in (S29) and (S31). Phase correlations are

$$g^{(1)}(z) = \exp \left\{ -\frac{1}{n} \int_{-\infty}^{\infty} \frac{dk}{2\pi} [(\bar{u}_k + \bar{v}_k)^2 n_k + \bar{v}_k^2] (1 - \cos kz) \right\}. \quad (\text{S34})$$

Since the density in  $k$  space can be expressed as  $\tilde{n}(k) = \frac{N}{2\pi} \int_{-\infty}^{\infty} dz g^{(1)}(z) e^{ikz}$ , (S34) can also be used to obtain the occupation of the lowest energy ( $k \rightarrow 0$ ) state:

$$N_0 = \tilde{n}(0)\Delta k = n \int_{-\infty}^{\infty} dz g^{(1)}(z). \quad (\text{S35})$$

The kinetic energy per particle is

$$\varepsilon = \frac{\hbar^2}{2mn} \int_{-\infty}^{\infty} \frac{dk}{2\pi} k^2 [(1 + 2\bar{v}_k^2) n_k + \bar{v}_k^2] \quad (\text{S36})$$

and  $\mathcal{E}_{\text{tot}} = \mathcal{E}_{\text{int}} + \varepsilon$ .

### C. Equivalent c-field description

The equilibrium c-field approximation corresponding to this is easily constructed. There are two changes:

1. The  $k$  values are restricted by the cutoff to lie in the range  $0 < |k| \leq k_c$ .
2. The operators  $\hat{b}_k$  are replaced by appropriate random complex numbers  $b_k$ , and  $\hat{P}$  can also be replaced by random real values  $P$  with variance  $k_B T \frac{L}{g}$ .

Applying the above changes, (S26) transform to:

$$\begin{aligned} \delta\hat{\rho}(x) &\rightarrow \frac{\sqrt{L\rho_0}}{2\pi} \int_{-k_c}^{k_c} dk (\bar{u}_k + \bar{v}_k) [e^{ikx} b_k + e^{-ikx} b_k^*] + \frac{P}{L} \\ \hat{\theta}(x) &\rightarrow \frac{\sqrt{L}}{4i\pi\sqrt{\rho_0}} \int_{-k_c}^{k_c} dk (\bar{u}_k - \bar{v}_k) [e^{ikx} b_k - e^{-ikx} b_k^*] - Q \end{aligned} \quad (\text{S37})$$

in the thermodynamic limit. The change from operators to c-numbers  $b$  requires some care. Firstly, now  $b$  and  $b^*$  commute, so that some observable expressions in thermal equilibrium need to be slightly modified (see below). This is achieved by deriving them according to the procedure of [87] but using (S37).

Also, since we want to compare c-field equilibrium to the quantum equilibrium state, we should remember that c-fields equilibrate to Rayleigh-Jeans occupations, not Bose-Einstein. Then, the thermal averages are  $\langle b_k^* b_{k'} \rangle = \delta_{kk'} n_k^{(\text{cf})}$ , with

$$n_k^{(\text{cf})} = \frac{k_B T}{E_k}. \quad (\text{S38})$$

and  $\langle b_k b_{k'} \rangle = 0$ . Here  $\langle \cdot \rangle$  now denotes stochastic averages over the random variables  $b$ . Means such as  $\langle b_k \rangle$  and  $\langle P \rangle$  remain zero.

The equation of state becomes

$$n = \frac{\mu}{g} - \int_{-k_c}^{k_c} \frac{dk}{2\pi} (\bar{u}_k + \bar{v}_k)^2 n_k^{(\text{cf})}. \quad (\text{S39})$$

We need to remember that now, similarly as in the numerical treatment of Sec. S1, the chemical potential for a given density  $n$  is different than the quantum one, and depends on the cutoff. That is,  $\mu \rightarrow \mu^{(\text{cf})}(k_c)$  when evaluating  $\bar{u}_k, \bar{v}_k, n_k^{(\text{cf})}$  or  $E_k$ .

Other observables turn out to be:

$$g^{(2)}(z) = 1 + \frac{2}{n} \int_{-k_c}^{k_c} \frac{dk}{2\pi} (\bar{u}_k + \bar{v}_k)^2 n_k^{(\text{cf})} \cos kz. \quad (\text{S40})$$

$u_G$  is now obtained via (9) to be

$$u_G = 2 \lim_{k \rightarrow 0} (\bar{u}_k + \bar{v}_k)^2 n_k^{(\text{cf})} = \frac{k_B T}{\mu^{(\text{cf})}(k_c)}. \quad (\text{S41})$$

This is the same convenient form as in (S41). Phase correlations are

$$g^{(1)}(z) = \exp \left\{ -\frac{1}{n} \int_{-k_c}^{k_c} \frac{dk}{2\pi} (\bar{u}_k + \bar{v}_k)^2 n_k^{(\text{cf})} (1 - \cos kz) \right\} \quad (\text{S42})$$

and  $N_0$  continues to be given by (S35) using this c-field  $g^{(1)}(z)$ . The interaction energy per particle continues to be (S33) and the kinetic energy is now

$$\varepsilon = \frac{\hbar^2}{2mn} \int_{-k_c}^{k_c} \frac{dk}{2\pi} k^2 (1 + 2\bar{v}_k^2) n_k^{(\text{cf})}. \quad (\text{S43})$$

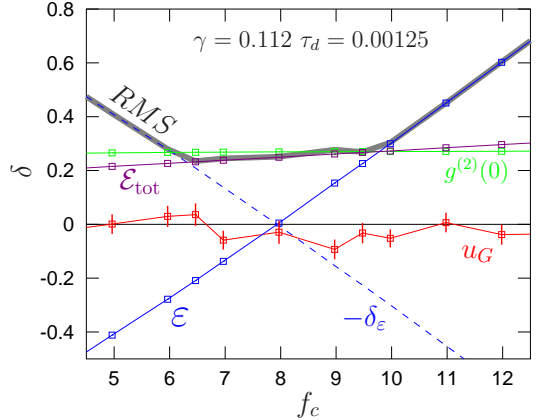


Figure S3. Cutoff dependence of the discrepancies  $\delta$  of single observables for the case  $\gamma = 0.112, \tau_d = 0.00125$ . Notation as in Fig. 1(a). The symbols show results obtained numerically with the SGPE (S8). The figure of merit  $RMS(f_c)$  is shown as the thick grey line. Error bars are shown for  $\delta_{u_G}$ , while the remaining error bars are below resolution. The dashed blue line shows  $-\delta_\varepsilon$  as a reference.

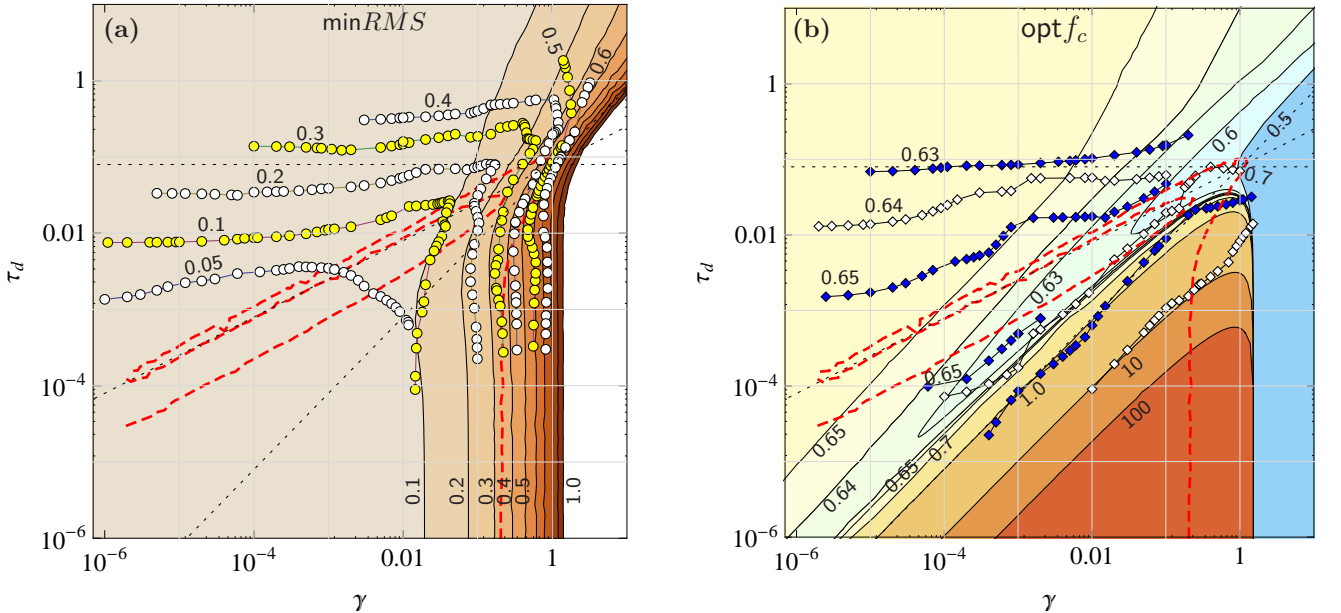


Figure S4. A detailed comparison of raw Bogoliubov and numerical ensemble results. Contours of  $\text{minRMS}$  (a) and  $\text{opt}f_c$  (b) are shown with numbered values on the plot, similarly to Figs. 2 and 4, respectively. Bogoliubov results are shown as solid contours between colored fields, while contours derived from the numerical ensembles presented in Fig. S1 are shown as joined symbols. Some random error in the numerical ensemble contours is present due to statistical noise and sparsity of data, especially near  $\gamma \sim \tau_d \sim 10^{-4}$  for  $\text{opt}f_c$ . The red dashed line is copied from Fig. S2 and shows the location at which the error between the Bogoliubov and exact results reaches 10%. The match between Bogoliubov and numerical contours in the region of applicability is remarkably good.

#### S4. CALCULATION OF OPTIMAL CUTOFF, FIGURE OF MERIT, AND CONTOUR DIAGRAMS

##### A. Processing of $\text{RMS}(f_c)$

For numerically generated ensembles, the set of data we use has been described in Sec. S1 A: about 10-15 c-field ensembles of  $\Psi(x)$  generated for different cutoff values  $f_c$  but the same  $\mu$ , as shown in Figs. 1(a) and S3 for high and low  $\gamma$ , respectively. The target was to obtain a resolution that is sufficient to determine  $\text{minRMS}$  and  $\text{opt}f_c$  to a satisfactory degree. To match these ensembles, exact quantum results were obtained using the Yang-Yang theory, but now with a  $\mu_Q(f_c)$  chosen individually for each  $f_c$  to obtain the required density  $n^{(\text{cf})}(f_c)$ . For each value of  $f_c$ , observable discrepancies  $\delta_\Omega$  were calculated according to (6) for all our observables. The values of  $\text{RMS}(f_c)$  were calculated using (8) from the values of  $\delta_\varepsilon$ ,  $\delta_{\varepsilon_{\text{tot}}}$  and  $\delta_{u_G}$ . These were all then inspected on plots like those shown in Figs. 1 and S3.

For Bogoliubov ensembles, the procedure is similar but simpler — it is a matter of computing several integrals and collecting the values into (8). As above, c-field values of observables  $\Omega^{(\text{Bog}-\text{cf})}$  are obtained for various  $f_c$ , and corresponding exact quantum values  $\Omega^{(\text{Bog}-\text{q})}$  obtained after matching the quantum density to that of the c-field. Observable and  $\text{RMS}(f_c)$  plots like Figs. 3 are inspected.

For both types of data, the approach taken to identify

$\text{opt}f_c$  depends now on the behavior of the minimum of  $\text{RMS}(f_c)$ .

A *rounded minimum* occurs when the interaction energy has only a minor contribution near  $\text{opt}f_c$ . Behavior of this kind is seen in Fig. 1. It happens typically in the hotter part of parameter space when thermal fluctuations dominate and  $\gamma$  is relatively small (it was already seen in the ideal gas [69]). Both  $\delta_{u_G}$  and  $\delta_\varepsilon$  are approximately linear in the region near the minimum of  $\text{RMS}$ , whereas  $\delta_{\varepsilon_{\text{tot}}} \approx \delta_\varepsilon$ . Then  $(\text{RMS})^2$  is given approximately by a sum of two parabolas — i.e. a parabola in  $f_c$ . Accordingly, we make a least squares fit of the numerical values of  $\text{RMS}$  to the parabola

$$\text{RMS}(f_c)^2 = a(f_c - \text{opt}f_c)^2 + (\text{minRMS})^2. \quad (\text{S44})$$

with fitting parameters  $\text{opt}f_c$ ,  $\text{minRMS}$  and  $a$  in the vicinity of the minimum. Examples are seen in Fig. 1(b). The fitted  $\text{opt}f_c$  and  $\text{minRMS}$  are our final estimates.

The other possibility is a *flat-bottomed minimum* like that noted in Fig. 3(c), and seen more clearly in Fig. S3. This occurs when the error in  $g^{(2)}(0)$  (and by implication in  $\mathcal{E}_{\text{int}}$  and  $\mathcal{E}_{\text{tot}}$ ) is sufficiently large near the minimum to compete with or exceed the error in  $u_G$ . Then, in the region in which  $|\delta_\varepsilon| \leq |\delta_{\varepsilon_{\text{tot}}}|$ , the error in  $\varepsilon$  becomes negligible, and  $\text{RMS} = \sqrt{\delta_{u_G}^2 + \delta_{\varepsilon_{\text{tot}}}}$ . Both of these two remaining errors usually depend weakly on  $f_c$ , and a flat-bottomed minimum like that seen in Fig. S3 appears. We choose the smaller of the two  $\text{RMS}$  values at the “corners” of the flat-bottomed minimum that occur at

$\delta_\varepsilon = \delta_{\varepsilon_{\text{tot}}}$  as  $\text{minRMS}$ , and the corresponding value of  $f_c$  as  $\text{opt}f_c$ . Some rare intermediate cases, such as when the maximum error swaps between  $\delta_{u_G}$  and  $\delta_{\varepsilon_{\text{tot}}}$  within the flat-bottomed minimum are dealt with on a case-by-case basis after inspection of the plot of  $\text{RMS}(f_c)$ .

In the end, we obtain a value of  $\text{opt}f_c(\gamma, \tau_d)$  and  $\text{minRMS}(\gamma, \tau_d)$  for each location shown in Fig. S1, and on a significantly finer grid in the Bogoliubov region. The value of the density  $n$  at the nearest data point to the minimum was used to calculate the corresponding  $\gamma$  and  $\tau_d$ .

Representative plots of the variation of  $\text{minRMS}$  are shown in Fig. S5 to complement  $\text{opt}f_c$  shown in Fig. 5.

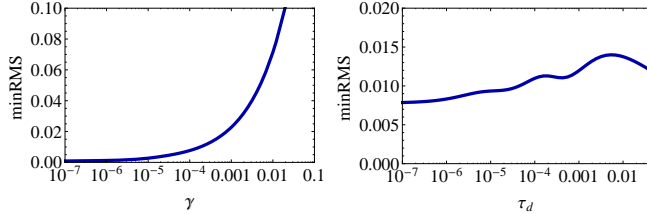


Figure S5. The dependence of  $\text{minRMS}$  in the Bogoliubov treatment for two characteristic sections of parameter space. Left panel:  $\tau_d = 10^{-6}$ . Right panel:  $\gamma = 1.2 \times 10^{-4}$ .

## B. Generation of contour diagrams

The raw results as separately obtained from numerical ensembles and Bogoliubov expressions are shown in detail in Fig. S4 in the form of contour diagrams.

The contours from numerical ensembles were obtained using Lagrangian interpolation of a function of two variables. Triangular polygons are successively selected using three corner points (labeled below as  $i = 1, 2, 3$ ), chosen from among those shown in Fig. S1. Within such a triangle, the interpolation of a function  $F$  that takes values  $F_i$  at the corner points is given by

$$F(\gamma, \tau_d) = \sum_j N_i(\gamma, \tau_d) F_i. \quad (\text{S45})$$

Here

$$N_i(\gamma, \tau_d) = \frac{1}{2A} (\alpha_i + \beta_i \gamma + \zeta_i \tau_d), \quad (\text{S46})$$

$A$  is the area of the triangle, and the coefficients are

$$\begin{aligned} \alpha_i &= \gamma_{i+1} \tau_{d,i+2} - \gamma_{i+2} \tau_{d,i+1} \\ \beta_i &= \tau_{d,i+1} - \tau_{d,i+2} \\ \zeta_i &= \gamma_{i+2} - \gamma_{i+1} \end{aligned} \quad (\text{S47})$$

where the indices  $i+1$  and  $i+2$  are understood as being modulo 3. The locus of a contour is obtained by requiring a given value of  $F$  (e.g.  $F = 0.1$ ) at chosen locations.

For the Bogoliubov case, the data was more finely spaced and smooth (no statistical errors due to finite ensemble size), and a simple application of the the Wolfram *Mathematica* algorithm `ContourPlot` turned out to be sufficient for the task.

Figures 2 and 4 show a distilled version of Fig. S4 that chooses the most accurate set of data for a given location in the diagram. The dashed red line in the background of Fig. S4 indicates  $\text{RMS}^Q = 0.1$ , and limits the region in which the Bogoliubov data can be considered accurate. Generally, we took the Bogoliubov contours below the lower red line, and the numerical ensemble data above. The ideal gas results are known from [69] and lie beyond the left of the diagrams. A straight line interpolation to them fits well with the numerical ensemble data.

A precise determination of the behavior of  $\text{opt}f_c$  in the salmon colored region of Fig. 4 proved elusive, however. The main contributing factor is that this is a region with only slight variation in  $\text{opt}f_c$  so that high precision is needed to locate the location of contours with spacing of only 0.01. Much larger numerical ensembles than those we generated would be necessary, as well as a finer spacing in  $\gamma, \tau_d$  parameter space. The Bogoliubov treatment no longer applies here, so provides no help.

What we can say is that the shallow valley seen for low  $\gamma, \tau$  appears to be real because it still remains in the regime of applicability of the Bogoliubov at very low  $\tau_d$ . It is not clear how far this valley survives as  $\gamma$  and  $\tau$  grow. While it is an intriguing feature, it does not hold much practical importance since a change of  $\pm 0.01$  in  $\text{opt}f_c$  does not affect the figure of merit,  $\text{RMS}$ , much. The salmon region for  $\gamma \gtrsim 0.1$  where uncertainty in  $\text{opt}f_c$  is larger is also of little practical importance since  $\text{minRMS}$  becomes large there and a c-field treatment is no longer recommended.

An overall point that should be emphasized is that the Bogoliubov and numerical ensemble contours agree very well in the region where both apply. Particularly notable is the agreement on the  $\text{opt}f_c = 10$  contour, which confirms the surprisingly rapid rise of  $\text{opt}f_c$  in the quantum fluctuating region using two very different methods.

## S5. KINETIC ENERGY AND CUTOFF IN THE QUANTUM FLUCTUATION REGION

Let us look into the reasons for the high globally optimal cutoff (11) in the quantum fluctuating regime. The exact Yang-Yang results for kinetic energy  $\varepsilon$  are shown in Fig. S6 and display a rapid increase once the regime  $\gamma \gtrsim 2\pi\tau_d$  is reached.

The reason for this rapid growth can be tracked to the kinetic energy present within the quantum fluctuations. To see this, let us make some coarse approximations to the Bogoliubov theory.

First, consider the thermal term in (S36) that contains  $n_k$ . The condition  $\mu \gg k_B T$  indicates that Bose occupations  $n_k$  begin to tail off exponentially well before ener-

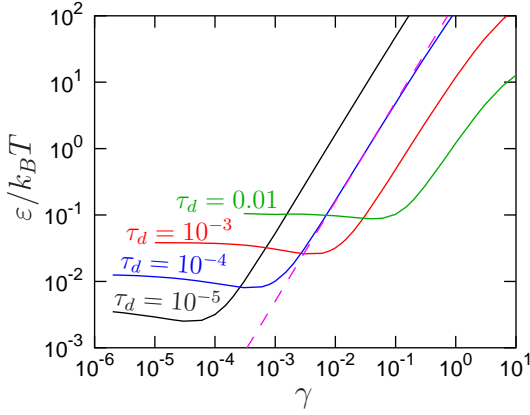


Figure S6. Kinetic energy  $\varepsilon$  as a function of  $\gamma$ . Exact Yang-Yang results. The magenta dashed line shows the approximation (S50) for  $\tau_d = 10^{-4}$ .

gies of the order of  $\mu$  are reached, and become negligible. Hence, to a zeroth approximation all the thermally relevant quasiparticle modes are in the phonon regime where  $E_k \approx \sqrt{2\varepsilon\mu} = \xi|k|\mu$ , and lie in the range  $|k| \lesssim k_B T/\mu\xi$ . In a second coarse simplification, the occupation of relevant modes that have  $E_k/k_B T \lesssim 1$  can be approximated by  $n_k \approx k_B T/E_k$ . Thirdly, the quantity  $\bar{v}_k^2 \approx 1/2\xi|k|$  in this regime is much greater than one. With all these, the thermal term in (S36) can be written as

$$\begin{aligned} \varepsilon_{\text{th}} &\approx \frac{\hbar^2}{2mn} \int_{-k_B T/\mu\xi}^{k_B T/\mu\xi} \frac{dk}{2\pi} k^2 \frac{1}{\xi|k|} \frac{k_B T}{\xi|k|\mu} = \left(\frac{k_B T}{\mu}\right)^2 \frac{\mu}{2\pi\xi n} \\ &\approx \frac{k_B T \tau_d}{\sqrt{\gamma}} \end{aligned} \quad (\text{S48})$$

The last result follows from  $\mu \approx gn = k_B T(\gamma/2\pi\tau_d)$ .

The quantum fluctuation term in (S36) contains just  $\bar{v}_k^2$  which switches to the rapidly decaying  $\bar{v}_k^2 \approx 1/(k\xi)^4$  in the particle regime once  $\varepsilon \gtrsim 2\mu$ . A coarse approximation is then to terminate the integral at the meeting point between these two trends at:  $|k| = 2^{1/3}/\xi$ , making the quantum fluctuation term as follows

$$\varepsilon_{\text{qf}} \approx \frac{\hbar^2}{2mn} \int_{-2^{1/3}/\xi}^{2^{1/3}/\xi} \frac{dk}{2\pi} k^2 \frac{1}{2\xi|k|} = \frac{\mu}{2^{5/3}\pi n \xi} \approx \frac{k_B T \gamma^{3/2}}{4\pi^2 2^{2/3} \tau_d} \quad (\text{S49})$$

This is far larger than (S48), and indicates that kinetic energy is indeed dominated by quantum fluctuations.

Bringing these approximations together, the kinetic energy per particle (S36) is estimated as

$$\varepsilon \approx k_B T \frac{\gamma^{3/2}}{4\pi^2 2^{2/3} \tau_d} = 0.016 k_B T \frac{\gamma^{3/2}}{\tau_d}. \quad (\text{S50})$$

(S50) captures the trend seen in Fig. S6, but also provides a very good estimate of the prefactor.

Let us now see what happens in the c-field description. The expression (S43) contains only a thermal term, but now there is no Gaussian decay of  $n_k^{(\text{cf})}$ . The limits

of integration of the thermal term will be different. In fact, since  $n_k^{(\text{cf})} = k_B T/E_k$ , we need to consider both the phonon-like and particle-like regimes.

Using again the crudest useful approximation, the phonon regime lies roughly in the range  $|k| \lesssim 2/\xi$ , where  $\bar{v}_k^2 \approx \frac{1}{2}(\frac{1}{\xi|k|} - 1) \gtrsim 1$  and  $n_k^{(\text{cf})} \approx k_B T/\xi|k|\mu$ . The particle-like regime has  $\bar{v}_k^2 \approx 1/(k\xi)^4 \ll 1$  and  $n_k^{(\text{cf})} \approx 2k_B T/\mu(\xi k)^2$ . Then,

$$\begin{aligned} \varepsilon^{(\text{cf})} &\approx \frac{\hbar^2}{mn} \left\{ \int_0^{2/\xi} \frac{dk}{2\pi} k^2 \frac{1}{\xi|k|} \frac{k_B T}{\xi|k|\mu} + \int_{2/\xi}^{k_c} \frac{dk}{2\pi} k^2 \frac{2k_B T}{\mu(\xi k)^2} \right\} \\ &= \frac{k_B T k_c}{\pi n} \left( 1 - \frac{1}{f_c} \sqrt{\frac{\mu}{2\pi k_B T}} \right) \\ &\approx \frac{k_B T k_c}{\pi n} = 2k_B T f_c \sqrt{\tau_d}, \end{aligned} \quad (\text{S51})$$

a remarkably simple result. The second term in the brackets on the 2nd line turns out to be small once the leading order estimate (S52) is obtained.

(S51) should be compared to the quantum kinetic energy (S50). Such comparison gives the following prediction for the cutoff

$$f_c \approx 0.008 \left( \frac{\gamma}{\tau_d} \right)^{\frac{3}{2}}. \quad (\text{S52})$$

This simple estimate agrees remarkably well with the Bogoliubov result (11) and the exact numerics.

The estimate (S51) corresponds to assuming exactly  $k_B T$  purely *kinetic* energy per mode. Since the vast majority of modes are particle-like because of the high cutoff, this is actually not an unreasonable approximation.

## S6. BOGOLIUBOV ESTIMATES FOR $\text{opt}f_c$ AND $\text{min}RMS$ IN THE QUANTUM FLUCTUATING REGIME

The quantum fluctuating Bogoliubov regime has two small parameters:  $\gamma \ll 1$  and a temperature scaled with respect to the chemical potential:

$$t = \frac{2\pi\tau_d}{\gamma} \approx \left( \frac{k_B T}{\mu} = u_G \right) \ll 1. \quad (\text{S53})$$

The equality  $k_B T/\mu = u_G$  follows from (S32) and (S41). We will make a self-consistent expansion of the required quantities in these small parameters. Further, we know empirically, approximately from Sec. S5, and will confirm retroactively from (S75) that the scaling  $\text{opt}f_c \propto t^{-3/2}$  holds in this regime. Hence, assuming that we will be working in the vicinity of  $\text{opt}f_c$  requires us to take this scaling into account in order to preserve terms of the right order in the expansion. Therefore, we define the prefactor  $p_c$  via

$$f_c = \frac{p_c}{t^{3/2}}. \quad (\text{S54})$$

### A. Chemical potential and related quantities

First we need to obtain an approximation to  $\mu$ . The equation of state (S29) can be evaluated as

$$\frac{1}{t} = \frac{1}{u_G} + \frac{1}{\pi} \sqrt{\frac{\gamma}{t u_G}} \left[ 1 - \frac{\pi^2 u_G^2}{12} + \frac{\pi^4 u_G^4}{48} - \frac{\pi^6 u_G^6}{32} + \mathcal{O}(u_G^8) \right]. \quad (\text{S55})$$

In detail, the integral in (S29) can be written

$$-\frac{T}{2\pi\sqrt{\mu}} \int_0^\infty ds \left[ \frac{s}{R(e^{sR\sqrt{2/u_G}} - 1)} + \frac{s - R\sqrt{2/u_G}}{2R} \right] \quad (\text{S56})$$

with  $R = \sqrt{1 + \frac{1}{2}s^2 u_G} = \sqrt{1 + \Delta(s)}$ . While the second term easily integrates to a closed form, the first does not. However, the  $[e^{sR\sqrt{2/u_G}} - 1]^{-1}$  factor cuts out any contributions at large  $s \gtrsim \sqrt{u_G/2}$ . These are small values, since  $u_G \ll 1$  in our regime. Further, this means that the quantity  $\Delta(s) = \frac{1}{2}s^2 u_G$  appearing in  $R$  takes on small values  $\Delta \lesssim \frac{1}{4}u_G^2 \ll 1$ , and that  $R \approx 1$ . Defining the deviation of  $R$  from unity as  $r = (R - 1) \ll 1$ , the first term in the integrand of (S56) can be written as a MacLaurin series in  $r$  indexed by  $j > 0$ . This leaves only exponential  $e^{s\sqrt{2/u_G}}$  components in the integral and no Gaussians. It turns out that integration is still troublesome beyond the lowest terms because of the square root dependence of  $r(s)$ , but we can further expand  $r = \frac{s^2 u_G}{4} - \frac{s^4 u_G^2}{32} + \dots$  to give the series

$$-\frac{T}{2\pi\sqrt{\mu}} \sum_{jj'>0} \int_0^\infty ds \mathcal{T}_{jj'}(s) \left( \frac{s^2 u_G}{4} \right)^{j'} + \frac{\sqrt{\gamma}}{\pi\sqrt{t u_G}}, \quad (\text{S57})$$

in which all the integrals can be evaluated in closed form and give (S55). We spare the reader from explicit expressions for the  $\mathcal{T}_{jj'}$ .

Now, to obtain a self-consistent expansion of  $\mu$ , we postulate an ansatz

$$\mu = \frac{k_B T}{t} \sum_{j,j' \geq 0} c_{jj'} t^j \gamma^{j'/2} \quad (\text{S58})$$

with coefficients  $c_{jj'}$  to be determined. By equating subsequent terms of the same orders of  $\sqrt{\gamma}$  and  $t$  appearing in (S29) one obtains the following series expansion:

$$\frac{\mu}{k_B T} = \frac{1}{t} \left[ 1 - \frac{\sqrt{\gamma}}{\pi} + \frac{\gamma}{2\pi^2} - \frac{\gamma\sqrt{\gamma}}{8\pi^3} \right] + \frac{t\sqrt{\gamma}\pi}{12} \left[ 1 + \frac{\sqrt{\gamma}}{\pi} + \frac{3\gamma}{8\pi^2} \right] \mathcal{O}(t^3, \gamma^2). \quad (\text{S59})$$

For c-fields, the integral in (S39) can be evaluated:

$$\frac{1}{t} = \frac{1}{u_G^{(\text{cf})}} - \frac{\sqrt{\gamma t u_G^{(\text{cf})}}}{\pi} \tan^{-1} \left[ f_c \sqrt{\frac{\pi u_G^{(\text{cf})}}{2}} \right], \quad (\text{S60})$$

and the resulting series expansion is

$$\begin{aligned} \frac{\mu^{(\text{cf})}}{k_B T} = & \frac{1}{t} + \frac{\sqrt{\gamma}}{2} \left[ 1 - \frac{t\sqrt{8}}{p_c \pi^{3/2}} + \frac{4t^3\sqrt{2}}{3\pi^{5/2} p_c^3} \right] - \frac{\gamma t}{8} \left[ 1 - \frac{t\sqrt{8}}{\pi^{3/2} p_c} \right] \\ & + \frac{5\gamma^{3/2} t^2}{64} \left[ 1 - \frac{8\sqrt{8}t}{5\pi^{3/2} p_c} \right] + \mathcal{O}(t^4, \gamma^2). \end{aligned} \quad (\text{S61})$$

Comparing the leading correction terms in (S59) and (S61), of  $\mathcal{O}(\sqrt{\gamma})$ , reveals immediately that they have the opposite sign, and no cutoff dependence. This proves what we previously found empirically – that no cutoff choice will match chemical potentials exactly in this regime. Since all of  $u_G$ ,  $\mathcal{E}_{\text{int}} = T/u_G - T/2t$  and  $g^{(2)}(0) = 2t\mathcal{E}_{\text{tot}}/T = (2t/u_G) - 1$  depend simply on  $\mu$  and the control parameters  $\gamma$  and  $\tau_d$ , they will also *never be exactly matched* by any cutoff. The leading order terms for the various observable estimates (which may be of use for future work) are:

$$u_G = t \left[ 1 + \frac{\sqrt{\gamma}}{\pi} + \frac{\gamma}{2\pi^2} \right] - \frac{\pi t^3 \sqrt{\gamma}}{12} \left[ 1 + \frac{3\sqrt{\gamma}}{\pi} \right] + \mathcal{O}(t^5, t\gamma^{3/2}) \quad (\text{S62})$$

$$u_G^{(\text{cf})} = t - \frac{t^2 \sqrt{\gamma}}{2} + t^3 \left[ \frac{\sqrt{2\gamma}}{\pi^{3/2} p_c} + \frac{3\gamma}{8} \right] + \mathcal{O}(t^4, \gamma^2) \quad (\text{S63})$$

$$\begin{aligned} g^{(2)}(0) = & 1 - \frac{2\sqrt{\gamma}}{\pi} + \frac{\gamma}{\pi^2} - \frac{\gamma^{3/2}}{4\pi^3} + \frac{\pi t^2 \sqrt{\gamma}}{6} \left[ 1 + \frac{\sqrt{\gamma}}{\pi} \right] \\ & + \mathcal{O}(t^4, t^2\gamma^{3/2}, \gamma^2) \end{aligned} \quad (\text{S64})$$

$$\begin{aligned} g^{(2)}(0)^{(\text{cf})} = & 1 + t\sqrt{\gamma} - t^2 \sqrt{\gamma} \left[ \frac{\sqrt{8}}{\pi^{3/2} p_c} + \frac{\sqrt{\gamma}}{4} \right] \\ & + t^3 \gamma \left[ \frac{1}{\sqrt{2}\pi^{3/2} p_c} + \frac{5\sqrt{\gamma}}{32} \right] + \mathcal{O}(t^4, \gamma^2). \end{aligned} \quad (\text{S65})$$

The discrepancy in  $u_G$  is

$$\begin{aligned} \delta_{u_G} = & -\frac{\sqrt{\gamma}}{\pi} + \frac{\gamma}{2\pi^2} - \frac{t\sqrt{\gamma}}{2} \left[ 1 - \frac{\sqrt{\gamma}}{\pi} \right] \\ & + t^2 \sqrt{\gamma} \left[ \frac{\pi}{12} + \frac{\sqrt{2}}{\pi^{3/2} p_c} \right] + t^2 \gamma \left[ \frac{11}{24} - \frac{\sqrt{2}}{\pi^{5/2} p_c} \right] + \mathcal{O}(t^3, \gamma^{3/2}) \end{aligned} \quad (\text{S66})$$

and in  $g^{(2)}(0)$ :

$$\begin{aligned} \delta_{g^{(2)}(0)} = & \frac{2\sqrt{\gamma}}{\pi} + \frac{3\gamma}{\pi^2} + t\sqrt{\gamma} \left[ 1 + \frac{2\sqrt{\gamma}}{\pi} \right] \\ & - t^2 \sqrt{\gamma} \left[ \frac{\pi}{6} + \frac{\sqrt{8}}{\pi^{3/2} p_c} \right] + t^2 \gamma \left[ \frac{13}{12} + \frac{4\sqrt{2}}{\pi^{5/2} p_c} \right] + \mathcal{O}(t^3, \gamma^{3/2}). \end{aligned} \quad (\text{S67})$$

### B. Kinetic energy

The integral (S36) can be reduced to integrable terms similar to (S57) in the same way as the one in (S29).

Upon substituting (S59) and keeping consistent orders, we obtain

$$\frac{\varepsilon}{k_B T} = \frac{\sqrt{\gamma}}{3\pi t} \left[ 1 - \frac{3\sqrt{\gamma}}{2\pi} + \frac{9\gamma}{8\pi^2} + \frac{\pi^2 t^2}{4} \left( 1 + \frac{\sqrt{\gamma}}{\pi} + \frac{3\gamma}{8\pi^2} \right) \right] + \mathcal{O}(t^3, \gamma^2). \quad (\text{S68})$$

The integral in (S43) can be performed, and

$$\frac{\varepsilon^{(\text{cf})}}{k_B T} = \sqrt{\frac{2\gamma t}{\pi}} \left( f_c - \frac{1}{\sqrt{2\pi u_G^{(\text{cf})}}} \tan^{-1} \left[ f_c \sqrt{\frac{\pi u_G^{(\text{cf})}}{2}} \right] \right). \quad (\text{S69})$$

This leads to the following expressions:

$$\frac{\varepsilon^{(\text{cf})}}{k_B T} = \frac{p_c \sqrt{2\gamma}}{t \sqrt{\pi}} - \frac{\sqrt{\gamma}}{2} + \frac{t \sqrt{2\gamma}}{\pi^{3/2} p_c} - \frac{t\gamma}{8} + \frac{3t^2\gamma}{p_c \sqrt{8\pi^{3/2}}} + \mathcal{O}(t^3, t^2\gamma^{3/2}, \gamma^2) \quad (\text{S70})$$

with the discrepancy

$$\delta_\varepsilon = 3p_c \sqrt{2\pi} - 1 + \frac{9p_c \sqrt{\gamma}}{\sqrt{2\pi}} + \frac{27p_c \gamma}{4\sqrt{2\pi^{3/2}}} - t^2 \frac{3(p_c^2 \pi^3 - 4)}{p_c \sqrt{8\pi}} - \frac{3\pi t}{2} \left[ 1 + \frac{3\sqrt{\gamma}}{2\pi} + \frac{9\gamma}{8\pi^2} \right] + \mathcal{O}(t^2 \sqrt{\gamma}, \gamma^{3/2}, t^3). \quad (\text{S71})$$

Equating this to zero gives the optimum cutoff for kinetic energy (only):

$$f_c^{(\varepsilon)} = \frac{1}{3\sqrt{2\pi} t^{3/2}} \left[ 1 - \frac{3\sqrt{\gamma}}{2\pi} + \frac{9\gamma}{8\pi^2} + \frac{3\pi t}{2} - t^2 \left( \frac{\pi^2 - 72}{4} \right) + \mathcal{O}(t^2 \sqrt{\gamma}, \gamma^{3/2}) \right] \quad (\text{S72})$$

One can see that the leading factor has the same  $t^{-3/2}$  dependence as (S52), and when converted to  $\gamma, \tau_d$  variables becomes  $f_c^{(\varepsilon)} = \frac{1}{12\pi^2} (\gamma/\tau_d)^{3/2} (1 + \dots)$ . The prefactor  $\frac{1}{12\pi^2} = 0.00844$  is a remarkably close match to that seen in (S52). To get the corrections correct and an estimate for  $\text{minRMS}$ , though, analysis of the full  $\text{RMS}$  figure of merit is necessary.

### C. Optimal cutoff

The discrepancy for total energy is

$$\delta_{\varepsilon_{\text{tot}}} = \sqrt{\gamma} \left[ \frac{4}{3\pi} + 2p_c \sqrt{\frac{2}{\pi}} - \frac{\pi t^2}{3} \right] + \gamma \left[ \frac{16}{9\pi^2} + \frac{8\sqrt{2}p_c}{3\pi^{3/2}} \right] - t^2 \gamma \left( \frac{31}{18} + \frac{2p_c \sqrt{2\pi}}{3} \right) + \mathcal{O}(t^3, \gamma^{3/2}). \quad (\text{S73})$$

Zeroing out the leading term requires negative  $p_c$ . This lets us conclude that  $\delta_{\varepsilon_{\text{tot}}}$  is always positive in the vicinity of the optimum cutoff that interests us, since  $p_c$  is postulated to be  $\mathcal{O}(1)$ . In fact,  $\delta_{\varepsilon_{\text{tot}}} \approx 2\sqrt{\gamma}/\pi$  at the  $f_c^{(\varepsilon)}$

cutoff, which we expect to be close to  $\text{minRMS}$ . This is equal to the leading term of the simple estimate (19).

As a corollary to the above, the term  $\mathcal{M} = \max[\delta_\varepsilon^2, \delta_{\varepsilon_{\text{tot}}}^2]$  in (8) must take on the flat-bottomed shape seen in Fig. 3(c). The ends of the flat-bottomed part will occur when  $\delta_{\varepsilon_{\text{tot}}} = \pm\delta_\varepsilon$ , i.e when

$$f_c^\pm = \frac{1}{3\sqrt{2\pi} t^{3/2}} \left[ 1 + \frac{(\pm 4 - 3)\sqrt{\gamma}}{2\pi} + \frac{(59 \mp 32)\gamma}{24\pi^2} + \frac{3\pi t}{2} \pm t\sqrt{\gamma} + \frac{(4 \mp 1)\gamma t}{6\pi} + \mathcal{O}(\gamma^{3/2}, t^2) \right]. \quad (\text{S74})$$

When the full  $\text{RMS}(f_c)$  in the flat bottom region is constructed, we have  $\text{RMS}^2 = \delta_{u_G}^2 + \delta_{\varepsilon_{\text{tot}}}^2 = \gamma(\frac{25}{9\pi^2} + \frac{16\sqrt{2}p_c}{3\pi^{3/2}} + \frac{8p_c^2}{\pi} + \mathcal{O}(t, \sqrt{\gamma}))$ . The leading order of this always has positive gradient with  $f_c$ , which implies that it is the leftmost edge that corresponds to the overall minimum of  $\text{minRMS}$ , i.e.  $\text{opt}f_c = f_c^-$ ,

$$\text{opt}f_c = \frac{1}{3\sqrt{2\pi} t^{3/2}} \left[ 1 - \frac{7\sqrt{\gamma}}{2\pi} + \frac{91\gamma}{24\pi^2} + \frac{3\pi t}{2} - t\sqrt{\gamma} + \frac{5\gamma t}{6\pi} + \mathcal{O}(t^2, \gamma^{3/2}) \right]. \quad (\text{S75})$$

The global figure of merit at this point is

$$\text{minRMS} = \frac{\sqrt{5\gamma}}{\pi} \left[ 1 + \frac{\sqrt{\gamma}}{30\pi} + \frac{\pi t}{2} + \frac{\sqrt{\gamma}t}{6} - t^2 \left( 6 + \frac{\pi^2}{12} \right) + \gamma \frac{1889}{1800\pi} + \mathcal{O}(t\gamma, t^2\sqrt{\gamma}, \gamma^{3/2}, t^2) \right]. \quad (\text{S76})$$

The leading orders of these are (11) and (12).